* Manuscript

A deformed alkaline igneous rock – carbonatite complex from the Western Sierras Pampeanas, Argentina: evidence for late Neoproterozoic opening of the Clymene Ocean?

C. Casquet[a*], R.J. Pankhurst[b], C. Galindo[a], C. Rapela[c], C.M. Fanning[d], E. Baldo[e], J. Dahlquist[e], J.M. González Casado[f†] F. Colombo[e]

[a] Dpto. Petrología y Geoquímica, Fac.Ciencias Geológicas, Inst. Geología Económica. (CSIC, Universidad Complutense), 28040 Madrid, Spain

[b] British Geological Survey, Keyworth, Nottingham NG12 5GG, UK

[c] Centro de Investigaciones Geológicas, Universidad de La Plata, 1900, La Plata, Argentina.

[d] Research School of Earth Sciences, The Australian National University, Canberra, ACT 200, Australia.

[e] CICTERRA (Conicet-Universidad Nacional de Córdoba), Vélez Sarfield 1611, 5016 Córdoba, Argentina.

[f] Dpto. de Geología y Geoquímica, Universidad Autónoma, 28049 Madrid, Spain.

† deceased

- *Corresponding author. Tel. +34 913944908; fax: +34 91
- E-mail address: casquet@geo.ucm.es

Abstract

A deformed ca. 570 Ma syenite–carbonatite body is reported from a Grenville-age (1.0 - 1.2 Ga) terrane in the Sierra de Maz, one of the Western Sierras Pampeanas of Argentina. This is the first recognition of such a rock assemblage in the basement of the Central Andes. The two main lithologies are coarse-grained syenite (often nepheline-bearing) and enclave-rich fine-grained foliated biotite-calcite carbonatite. Samples of carbonatite and syenite yield an imprecise whole rock Rb–Sr isochron age of 582 ± 60 Ma (MSWD = 1.8; Sri = 0.7029); SHRIMP U–Pb spot analysis of syenite zircons shows a total range of ^{206}Pb–^{238}U ages between 433 and 612 Ma, with a prominent peak at 560–580 Ma defined by homogeneous zircon areas. Textural interpretation of the zircon data, combined with the constraint of the Rb–Sr data suggest that the carbonatite complex formed at ca. 570 Ma. Further disturbance of the U–Pb system took place at 525 ± 7 Ma (Pampean orogeny) and at ca. 430 – 440 Ma (Famatinian orogeny) and it is concluded that the Western Sierras Pampeanas basement was joined to Gondwana during both events. Highly unradiogenic ^{87}Sr/^{86}Sr values in calcites (0.70275 – 0.70305) provide a close estimate for the initial Sr isotope composition of the carbonatite magma. Sm–Nd data yield εNd_{570} values of +3.3 to +4.8. The complex was probably formed during early opening of the Clymene Ocean from depleted mantle with a component from Meso-/Neoproterozoic lower continental crust.

Keywords: DARCs; Syenite; U-Pb SHRIMP zircon dating; Gondwana; Rodinia.

Introduction

The association of alkaline igneous rocks (particularly nepheline syenites) with carbonatites is common in continental rift settings (Bailey, 1977, 1992; Bell, 1989; Burke et al., 2003), where they are sometimes referred to by the acronym ARCs (Alkaline Rock – Carbonatite complexes). Deformed, i.e., variably foliated concordant lenses (DARCs) are a special case, in which they apparently match ancient sutures in basement regions (Burke et al., 2003). Since sutures are indicative of orogenic continental collision at the end of a Wilson cycle, one interpretation of these deformed rock associations is that they represent earlier rift-related ARC assemblages that eventually became involved in the collision zone (Burke and Khan, 2006). An alternative interpretation, based on geochronological constraints, is that they formed during syn-orogenic extension related to continental orogeny, e.g., along the Dahomeyide suture zone of western Africa (Attoh et al., 2007). In a recent synthesis of the many 650–500 Ma alkaline rocks and carbonatites related to the amalgamation of Gondwana, Veevers (2003, 2007) favoured the location of these and other alkaline associations at releasing bends along transcurrent faults driven by collisional oblique stresses and during post-collisional relaxation. Vaughan and Scarrow (2003) outlined a model for the generation of potassic mafic and ultramafic magmas by transtension of metasomatized mantle.

We describe here the case of a Neoproterozoic deformed syenite – carbonatite body intruded into a Grenville-age (1.0 – 1.2 Ga) terrane in the Sierra de Maz, one of the Western Sierras Pampeanas of Argentina. After Rodinia break-up this terrane was involved in an Early Paleozoic collision, the Pampean orogeny, a stage in the amalgamation of SW Gondwana that involved subduction-related granite magmatism and high-grade metamorphism, largely to the east of the Western Sierras Pampeanas (Rapela et al., 2007). It is thus is a good test case for geotectonic models for deformed ARC formation. Moreover, to our knowledge this is the first recognition of such a rock assemblage of Precambrian age in the basement of the Central

Andes, which could prove to be of economic importance. Carbonatite and a diversity of alkaline silicate rocks and related hydrothermal alteration products of Cretaceous age are however well known from elsewhere in the Central Andes and its eastern foreland (e.g., Schultz et al., 2004, and references therein). Geochronological constraints and isotope geochemistry suggest that the first mode of deformed ARC formation above, i.e. early during the Pampean Wilson cycle in the late Neoproterozoic, probably applies in the case of the Maz syenite – carbonatite body. Moreover syenite and carbonatite magmas were coeval and were mainly fed from a depleted mantle source, probably with a minor contribution from a poorly radiogenic continental crust of Grenville age.

Geological and paleogeographical setting

The Sierras Pampeanas of Argentina are elongated blocks of pre-Andean crystalline basement that were exposed to erosion by tilting during Cenozoic Andean tectonics (Fig. 1). Three metamorphic and igneous belts have been distinguished (for a review, see Rapela et al., 1998a, 2002) (Fig. 1a): (1) The older is of 'Grenville' age, ca. 1.0 to 1.2 Ga, and crops out in the Western Sierras Pampeanas. (2) The Pampean belt is of Early Cambrian age, between 530 and 515 Ma, and crops out in the Eastern Sierras Pampeanas. (3) The Famatinian belt of Ordovician age, ca. 490 to 430 Ma, is located between the former two and is the best preserved. Famatinian metamorphism, deformation and magmatism overprint with varied extent and intensity the Grenvillian and Pampean belts. The Sierra de Maz (Fig. 1b) is one of the Western Sierras Pampeanas where Grenville-age metamorphic and igneous rocks have been recognized (Porcher et al., 2004; Casquet et al., 2005, 2006, 2008). Other larger outcrops of Grenville-age rocks exist in the Sierra de Pie de Palo (see review by Ramos, 2004) and Umango (Varela et al., 2003) (Fig. 1).

Paleogeographic reconstructions and dynamic interpretations of the proto-Andean margin of Gondwana in the Mesoproterozoic to Ordovician time span have been strongly stimulated over the past fifteen years by the hypothesis of allochthoneity of the Precordillera terrane (e.g., Vaughan and Pankhurst, 2008). According to most supporters of the hypothesis, this terrane consists of a Grenville-age basement that crops out in the Western Sierras Pampeanas and a non-metamorphic Early Cambrian to Middle Ordovician passive margin cover sequence, i.e., the Argentine Precordillera (Fig. 1) (for reviews see Thomas and Astini, 2003; Ramos, 2004). In this paradigm, the Precordillera terrane is an exotic terrane rifted away from the Ouachita embayment in the Appalachian margin of eastern Laurentia in the Early Cambrian that collided with the proto-Andean margin of Gondwana in the Ordovician to produce the Famatinian orogeny (Thomas, 1991; Thomas and Astini, 1996). However, whether the Grenvillian outcrops in Western Sierras Pampeanas are part of the exotic terrane or not has also been questioned (Galindo et al., 2004; Rapela et al., 2005; Casquet et al., 2008). In a recent contribution Rapela et al. (2007) suggested that after initial break-up of Rodinia the Western Sierras Pampeanas Grenville-age basement was part of a larger continental mass embracing the Mesoproterozoic central and northern Arequipa–Antofalla craton (Peru), and the Amazonia craton (Brazil). These continental domains coalesced during the Sunsas (Grenville-age) orogeny (Loewy et al., 2004; Tohver et al., 2002, 2004; Casquet et al., 2008). This large continent collided obliquely with the Rio de la Plata and Kalahari cratons to the east (present coordinates) to produce the Pampean orogeny in the early Cambrian, with the disappearance of the intervening Clymene Ocean (Trindade et al., 2006).

Field description

The Maz deformed syenite–carbonatite complex forms a body ca. 4 km long and of variable thickness (max. 120 m), striking 340–345º along the eastern margin of the Sierra de

Maz and dipping 65–70º E. (Figs 2, 3a). Host rocks are: 1) hornblende-biotite-garnet gneisses and biotite-garnet gneisses with some interleaved quartzites and marbles, 2) ortho-amphibolites, metagabbros and local meta-peridotites; 3) massif-type anorthosites of 1070 ± 41 Ma (Casquet et al., 2005) and a variety of coeval granitic orthogneisses. Host rocks to the complex (Fig. 1b) belong to the Maz Central Domain (Casquet et al., 2008), which underwent granulite facies metamorphism at ca. 1.2 Ga and retrogression under amphibolite facies conditions at 431 ± 40 Ma (Casquet et al., 2006, 2008). The intrusion is largely concordant, but locally discordant, to the foliation of the host rocks (Fig. 2).

Homogeneous medium- to coarse-grained syenite and fine-grained foliated biotite carbonatite are the two main lithologies forming the body. They do not show a clear internal arrangement, syenite ranging from elongated bodies tens of metres long down to few centimetre-size spheroidal enclaves in the carbonatite. Carbonatite foliation wraps around the syenite bodies that are locally foliated as well (Fig. 3b). Besides syenite, the carbonatite hosts a number of other types of enclaves, notably large (up to several centimetres) isolated crystals of albite and biotite, coarse-grained mafic enclaves, and enclaves of the host gneisses and amphibolites with the internal foliation in places at a high angle to the carbonatite foliation (Fig. 3c). Enclaves are rounded to sub-angular and vary from well- to poorly-sorted in terms of size from place to place, and can be locally very abundant, giving the outcrop a breccia-like aspect (Fig. 3d). Enclaves of an earlier carbonatite (also with enclaves) can be found within a younger carbonatite. Variability in the number and sorting of the enclaves suggests that their incorporation in the carbonatite magma was a multi-stage process (Fig. 3e). The syenites contain visible pinkish zircon megacrysts that can attain few cm size (Fig. 3f), a feature also recognized in carbonatite – syenite bodies elsewhere (Ashwal et al., 2007). Coarse-grained calcite veins and interstitial calcite are locally found in syenites.

Petrography and mineralogy

The carbonatite consists of calcite, 10 to 30 % modal biotite, abundant anomalous biaxial apatite, and minor magnetite, zircon, very scattered U-rich pyrochlore, and columbite. Compositionally the calcite has up to 1.3 wt. % SrO, 2.5 wt. % FeO, and 0.41 wt. % ΣLREE (Table 1 and microprobe data in the data repository; see below). Electron microprobe analyses of the biotite show an average Fe# value [Fe/(Mg+Fe)] of 0.74 and Al^{IV} = 2.643–2.748 a.f.u.; the apatite has up to 2.76 wt. % F, the pyrochlore 18.60–30.23 wt. % UO_2 and the columbite Nb/Nb+Ta = 0.98. Calcite crystals are fine-grained granoblastic with a slight preferred orientation and narrow straight twins. Lattice-preferred orientation is weak but relics of larger strained crystals of calcite are preserved within the foliated granoblastic groundmass, suggesting that the latter probably arose by recrystallization of former coarser-grained, probably primary, carbonate crystals. Groundmass biotite is found as individual plates but more commonly as fine-grained recrystallized aggregates, often as rims on isolated rounded albite crystals or larger albite syenite spheroids. The visible foliation largely results from preferred orientation of biotite.

The syenites are coarse-grained rocks that are locally foliated. They consist of albite ($Ab_{95.0\text{-}97.5}An_{2.2\text{-}2.6}Or_{0.9\text{-}2.5}$) and biotite chemically similar to that in the carbonatite (Fe# = 0.83). Subordinate microcline is found at albite grain boundaries, as either replacement or exolution. Undulose extinction and deformation bands in albite, and bending and kinking in biotite, are common in non-foliated varieties. K-rich nepheline ($Ks_{21\text{-}22}$), variably converted to a fine-grained micaceous aggregate, was found in several samples. Accessory minerals are zircon, anomalous biaxial apatite and minor pyrochlore. Secondary minerals in the syenites are calcite, muscovite-sericite after K-feldspar and chlorite and epidote after biotite. Syenite spheroids within the carbonatite consist of an inner coarse-grained core and a continuous fine-grained mantle resembling a chilled margin, rimmed by fine-grained biotite, probably indicative of liquid inmiscibility. Foliated syenites are medium-grained and show a granoblastic orientation of albite and preferred orientation of biotite.

Besides large biotite and albite megacrysts, two types of mafic enclaves have been found in the carbonatite. One type consists of coarse-grained aegirine-augite (Na_2O = 5.35–5.75 wt. %) variably converted to katophorite amphibole, albite, Fe-rich calcite and magnetite. The second type consists of coarse-grained magnetite and biotite with accessory primary calcite (included in biotite), apatite and pyrochlore.

Analytical procedures

Full chemical analyses of four syenite and two carbonatite samples were performed at ACTLABS (Canada): major oxides by ICP and trace elements by ICP-MS. Other determinations at ACTLABS were Cl (INAA), CO_2 (COUL), F (FUS-ISE), and S (IR). Fe^{2+} was determined volumetrically at the Centro de Investigaciones Geológicas, La Plata. Major and trace elements of one probably relic calcite megacryst were determined by XRF (Table 1) and mineral compositions by electron microprobe at the Universidad Complutense, Madrid (Supplementary Table obtainable from the Precambrian Research Data Repository) .

Rb–Sr systematics were analysed in three samples of carbonatite, four of syenite, two vein calcites in syenites, and four enclaves in carbonatite – an aegirine mafic enclave (see below) and three megacrysts, two of biotite and one of albite. For Sm–Nd systematics five samples were analysed: two syenites and three carbonatites. Samples were crushed and powdered to ~ 200 mesh. For the carbonatite samples, Sr and Nd isotope composition was obtained by leaching 200 mg of each sample in10 ml of acetic acid for 12 hours. Whole-rock syenites and silicate minerals were first decomposed in 4 ml HF and 2 ml HNO_3, in Teflon digestion bombs during 48 hours at 120 ºC and finally in 6M HCl. Elemental Rb, Sr, Sm and Nd in carbonates and silicates were determined by isotope dilution using spikes enriched in ^{87}Rb,

^{84}Sr, ^{149}Sm and ^{150}Nd. Ion exchange techniques were used to separate the elements for isotopic analysis. Rb, Sr and REE were separated using Bio-Rad AG50 x 12 cation exchange resin. Sm and Nd were further separated from the REE group using Bio-beads coated with 10% HDEHP. All isotopic analyses were carried out on a VG Sector 54 multicollector mass spectrometer at the Geocronología y Geoquímica Isotópica Laboratory, Complutense University, Madrid, Spain. Isotope data are shown in Table 2. Errors in the initial ratios are reported at 2σ.

U-Th-Pb analyses were performed on two samples using SHRIMP II at the Research School of Earth Sciences, The Australian National University, Canberra. One was a euhedral zircon megacryst up to 1.5 cm in width, extracted from a syenite; the second was a hand-picked concentrate separated after milling another syenite. Zircon fragments were mounted in epoxy together with chips of the Temora reference zircon , ground approximately half-way through and polished. Reflected and transmitted light photomicrographs, and cathodo-luminescence (CL) SEM images, were used to decipher the internal structures of the sectioned grains and to target specific areas within the zircons. Each analysis consisted of 6 scans through the mass range. The data were reduced in a manner similar to that described by Williams (1998, and references therein), using the SQUID Excel Macro of Ludwig (2001). Data for the geochronology samples are given in Table 3.

Geochemistry

Major and trace elements

The syenitic rocks display a relatively wide, alkali-rich compositional range from nepheline monzosyenites (52% SiO_2) to normal syenites (58–64% SiO_2) (Table 1, Fig. 4), and are Na-rich (K_2O/Na_2O mol ≤ 0.33). They plot in the alkali and ferroan fields of the Frost et al. (2001) diagram, clearly indicating an alkaline signature for the parental magma (Figs 4b, 4c).

The Zr content of the suite is remarkably high (716–1920 ppm), consistent with experimental evidence indicating that Zr is more soluble in peralkaline than in metaluminous melts (Watson, 1979; Watson and Harrison, 1983). A negative correlation between Zr and Agpaitic Index (Fig. 5a) strongly suggests that the alkali content of the melt controlled the crystallization of zircon. Zircon saturation temperatures (T_{Zr}) calculated from bulk-rock compositions using the equations of Watson and Harrison (1983) and Miller et al. (2003), yield initial temperatures of crystallization between 826ºC and 1022ºC, similar to those recorded for basaltic magmas.

The syenitic suite shows a strong decrease in P_2O_5, REE_{total}, Sr and Y with SiO_2 (Fig. 6). REE patterns also change significantly with silica content, from $[La/Yb]_N$ = 26 in the least evolved rock, to a U-shaped pattern with $[La/Yb]_N$ = 2.33 and a well-developed positive Eu anomaly in the most evolved one (Fig. 7a). P_2O_5 contents decrease from 0.74% (1.9% normative apatite) in the least evolved syenite to 0.02% (0.05% normative apatite) in the most evolved one.

The REE pattern of the nepheline monzosyenite (MAZ-12110, Fig. 7a) might reasonably suggest control entirely by the modal content of apatite (Fig. 7b). However, the HREE distribution cannot be explained by fractionation of apatite alone, particularly in the rocks of intermediate composition, as the decreasing slope of the patterns suggests crystallization of a mineral phase with a high partition coefficient for HREE, such as zircon (Fig. 7a and b). As noted above, zircon is a conspicuous accessory mineral in the syenitic suite, with megacrysts up to a few cm in size. Coupled fractionation of apatite and zircon may replicate the observed REE patterns in the syenites of intermediate composition (SiO_2 = 58–61 %). The depletion of REE in the most evolved syenites (SiO_2 = 64%) may be explained by the effective fractionation of accessory minerals, leaving plagioclase-rich residual liquids (Fig. 7a and b).

The two carbonatite samples (Table 1) are silico-carbonatites that have steep, LREE-enriched patterns with no Eu anomalies, and plot within the field defined for most world-wide carbonatites (Fig. 7c). They also contain large amounts of Ti, Nb, Y, Sr and Ba (Table 1), as usually reported in carbonatite complexes (e.g., Culler and Graf, 1984). Compared with the carbonatite whole-rock REE patterns, the REE analysis by XRF of a relic large homogeneous crystal of calcite (Table 1, sample MAZ-12090), shows a parallel but slightly more enriched pattern (Fig. 7c). The REE pattern of the least evolved member of the syenitic suite (MAZ-12110) (Fig. 7a), has lower total REE content than associated carbonatites, but similar LREE/HREE ratios (Fig. 7c), a characteristic that has been reported in several alkaline-carbonatite complexes (e.g., Culler and Graf, 1984; Villenueve and Relf, 1998).

Rb–Sr and Sm–Nd Isotope Systematics

The present-day Sr isotope compositions of the carbonatite calcite and vein calcite are similar and very unradiogenic (Table 2). The slightly higher $^{87}Sr/^{86}Sr$ values in the carbonatite calcite (0.70299–0.70305) than in vein calcite (0.70275–0.70277) is probably due to very minor contamination of the carbonatite leachate with Sr derived from biotite. In all cases the very low $^{87}Rb/^{86}Sr$ ratios of the calcites resulting from the very high Sr contents (3108–8493 ppm), mean that the Sr isotope composition is almost invariant with age (Table 2) and the present values can thus be taken as a close estimate for the initial Sr isotope composition of the carbonatite magma at the time of formation, i.e., 0.7027 to 0.7030. When carbonatites and syenite data are plotted as $^{87}Rb/^{86}Sr$ *vs.* $^{87}Sr/^{86}Sr$, an isochron age of 582 ± 60 Ma (MSWD = 1.8; Sr_i = 0.7029) is obtained (Fig. 8). For this plot only syenites MAZ-12057 and MAZ-12085 were used because they do not show evidence of significant alteration of primary minerals (syenites MAZ-12058 and MAZ 12110 show deformation and strong alteration of nepheline and biotite). The albite megacryst and the aegirine mafic enclave both have high Sr contents (4211 and 3108 ppm, respectively) and low $^{87}Rb/^{86}Sr$ ratios (Table 2). When these data are included in the isochron dataset an indistinguishable age is obtained (565 ± 60 Ma, MSWD = 3.3, Sr_i = 0.70300). The two biotite megacrysts have model ages (assuming an initial $^{87}Sr/^{86}Sr$ of 0.703, of 490 ± 7 and 480 ± 11 Ma, indicating either late crystallization (or loss of radiogenic Sr) – see below. The very unradiogenic nature of the carbonate Sr isotope composition suggests a significant contribution to the magma from a depleted source.

Sm–Nd data (Table 2) yield epsilon values at the reference age of 570 Ma (εNd_{570}) between +3.3 and +4.8, also suggesting a major contribution to the Nd isotope composition of magma from a depleted mantle source. Nd model ages (T_{DM}*) between 764 and 986 Ma are significantly older than those obtained from the Rb–Sr data and zircon chronology (see below). The Sm–Nd data for the five analysed whole-rock do not fit an isochron (MSWD 10.2), suggesting that Sm-Nd systematics were perturbed after magmatic crystallization; chemical and geochronological evidence from zircon is consistent with this interpretation.

Zircon internal structure and U–Pb chronology

A feature of the syenite is the presence of euhedral mm-size pinkish zircon crystals, which has also been found in nepheline-syenite carbonatite complexes elsewhere (Ashwal et al., 2007). Megacrysts up to a few cm in size are also randomly distributed (Fig. 3f). Internal fractures are common. Back-scattered electron (BSE) images (Fig. 9a) show a complex zoning pattern probably resulting from post-crystallization modification. Light-coloured zones are enriched in Th, U and REE and are poorer in Hf compared to the darker ones.

Zircon megacryst,

One megacryst (MAZ-12089) was extracted in the field for initial study. Cathodo-luminescence (CL) images (Fig. 9b) show that it has a very complex internal structure. The oldest zircon in textural terms appears as internal areas of relatively uniform growth with low luminescence; there are also areas of higher luminescence and rather irregular alternating structure which are nevertheless relatively homogeneous. However, large irregular areas have variable luminescence with complex internal structure which appears to be secondary. Within the latter we distinguish areas of complex patchy texture, and areas in which highly luminescent microveins penetrate the old homogeneous zones, apparently resulting from replacement or recrystallization along cracks. Such complex textures are usually ascribed to late or post-magmatic processes, including hydrothermal alteration, and metamorphism (see Corfu et al., 2003, figures 6-16, 10-5 and 11-7). Finally, there is one peripheral area with more regular oscillatory zoning that could represent newer growth.

SHRIMP U–Pb spot analysis (Table 3a) shows that the structural complexity corresponds to a large extent with variable isotope systematics. The total range of apparent ^{206}Pb-^{238}U ages is 433–612 Ma, but most of the areas in relatively homogeneous domains yield ages of 530–590 Ma (e.g., Fig. 9b), with a single anomalous age of 612 Ma, whereas the mosaic areas generally yielded ages of <500 Ma. The outer oscillatory-zoned domain also yielded younger ages of 450–495 Ma (spots 1, 2, 3), clearly reflecting much later re-growth. Overall, there is no obvious correlation between age and either U content or Th/U ratio. Eight results from the most homogeneous areas (spots 5,6, 10, 12, 14, 14 and 16 in Table 3) gave a weighted mean age of 566 ± 8 Ma (MSWD 1.5) and three within the more complex areas (spots 9, 11 and 18) gave 530 ± 19 Ma (MSWD 1.4). These results are illustrated in a Tera-Wasserburg plot and a probability density diagram (Fig. 10a and 10b, respectively).

Groundmass Zircon

Zircon extracted from whole-rock crushing of syenite MAZ-12057 consists entirely of irregularly-shaped grains up to 500 μm in length of clear but heavily fractured zircon. The internal structure revealed by CL predominantly corresponds to the more homogenous type seen in the megacryst, albeit still with irregular cross-cutting zones with alternating structure (Fig. 9c). The absence of euhedral grains and the incomplete internal structures indicate that these grains are not individual crystals but fragments of larger grains, broken along internal fractures either in a geological event or during the mineral separation process. The latter is suggested by the occasional occurrence of mosaic patterned grains and is confirmed by examination of *in situ* zircon crystals in petrographic thin sections of other samples of the syenite (e.g., Fig. 9a) which show more complete zoned domains but extensive fractures.

The ^{206}Pb-^{238}U ages obtained from the fragmented grains of MAZ-12057 (Table 3b) are similar to those from the more homogeneous domains of the megacryst, ranging from 495 to 588 Ma (see Fig 11a, b). Even this more limited range is well outside the analytical uncertainty of the individual results and encompasses a distribution that is at least bi-modal, twenty-two of the ages clustering around a broad peak at 571 ± 5 Ma (albeit with MSWD =2.8) and a smaller group of five defining a weighted mean of 525 ± 7 Ma (MSWD = 0.2) and a single age at 495 Ma. As with the megacryst analyses there is no obvious relationship between age and parameters such as U content or Th/U ratio.

Discussion

The Maz outcrop is an example of a *deformed alkaline rock – carbonatite* complex. Beyond its potential economic importance (Nb, REE), this type of complex can be of value in constraining geodynamic and paleogeographic models of continental dispersal and amalgamation if the age of intrusion is defined.

Chronological interpretation and geodynamic implications

The Maz carbonatite – syenite was intruded into a Grenville-age basement that forms the central and eastern side of the sierra. The local obliquity of the body to the regional foliation and the fact that rotated blocks of the host gneisses are locally found in the carbonatite, together with the zircon U-Pb geochronological data presented here, show that its emplacement age is post-Grenvillian. In the absence of any textural indication of inheritance, it is most probable that the older zircon ages, yielding means of 566 ± 7 Ma in the case of the megacryst and 571 ± 5 Ma in that of the groundmass zircon, represent igneous crystallization during the Late Neoproterozoic. It is difficult to know whether the spread of the latter group indicated by the MSWD of 2.8 might signify more than one event; the most definitive statement that can be made concerning the age of this carbonatite complex is that it was emplaced within the interval 565–580 Ma, most probably at ca. 570 Ma, i.e., Ediacaran.

The Rb–Sr whole rock systematics reinforce this interpretation; the two calculated isochron ages (582 ± 60 Ma and 565 ± 60 Ma) are within error of the U–Pb zircon ages. The large uncertainties in these ages are due to the limited range of Rb/Sr ratios, and this might lead to some doubts over the confidence of this result. However, we note that the whole-rock Rb-Sr system in these rocks appears to have been resistant to disturbance during the amphibolite-facies Famatinian metamorphism and deformation at ca. 430–440 Ma, which affected the whole region (Lucassen and Becchio, 2003; Casquet et al., 2005, 2008). A significantly older maximum possible age for the carbonatite – syenite complex might be suggested by the Sm-Nd T_{DM}* model ages of 764–986 Ma, but in view of the fact that the whole-rock syenites do not yield a reasonable Sm–Nd isochron, these seem as likely to reflect metamorphic disturbance of the Sm–Nd systems in a carbonate-rich environment, where REE are known to be relatively mobile (McLennan and Taylor, 1979; Banner et al., 1988). Alternatively, pre-crystallization Sm–Nd systematics may reflect some crustal contribution to the magma.

Consequently we conclude that the Maz carbonatite – syenite complex is the first evidence of a Late Neoproterozoic rifting event in the Western Sierras Pampeanas.

In the case of the zircon megacryst it would be possible to interpret the few ages at ~520 Ma as due to partial Pb-loss. On the other hand, the well-defined age grouping at 525 ± 7 Ma given by zoned zircon in the whole-rock syenite, where Famatinian reworking is clearly minor (only one age of <500 Ma), seems to indicate a specific event related to rejuvenation at the time of the Pampean orogeny (Rapela et al., 1998b). The zoned zircon areas that yield this age are not texturally distinguishable from the older zircon (there is certainly no evidence for any core–rim relationship indicating re-growth), implying that these Pampean ages represent cryptic Pb-loss in a discrete event.

This interpretation of the ~525 Ma U–Pb zircon ages may be taken as further evidence of the effects of the Early Cambrian Pampean orogeny in the Western Sierras Pampeanas. Until now most reliable metamorphic ages in the Maz and Espinal area were either Grenville-age (ca. 1.2 Ga) or Famatinian (430–440 Ma, e.g., Lucassen and Becchio, 2003; Porcher et al., 2004; Casquet et al., 2005, 2006, 2008; and our unpublished data). Involvement of the Western Sierras Pampeanas Grenville-age basement in the Pampean orogeny has, however, been recently emphasized by Rapela et al. (2007). Recent determinations of a single U–Pb titanite age of ca. 530 Ma from the southern tip of the Sierra de Maz (Lucassen and Becchio, 2003) and of a metamorphic hornblende Ar-Ar age of ca. 515 Ma in the Grenvillian basement of the Sierra de Pie de Palo, south of Sierra de Maz (Mulcahy et al., 2007), strengthens this geodynamic interpretation.

According to the majority of the textural evidence, the younger ages of 433–495 Ma, particularly in the megacryst, are almost certainly related to minor zircon growth and variable Pb-loss, in part caused by invasive fluids penetrating along fractures, and would correspond to reactivation during Famatinian metamorphism. The highly fractured nature of the zircon megacryst would probably also have facilitated fluid exchange processes. Evidence for deformation and metamorphic rejuvenation under amphibolite facies conditions in the Maz and Espinal area at ca. 430 - 440 Ma has been shown by Lucassen and Becchio (2003), Porcher et al. (2004) and Casquet et al. (2005, 2008).

Tectonic implications

The rock association of alkali-syenite (+ nepheline) and carbonatite, with no evidence for associated alkali basalts shows that this is not a high-thermal anomaly mantle plume scenario, but was most probably related to an extensional environment. Vaughan and Scarrow (2003) suggested transtensional tectonics in a metasomatized mantle, but this produces K-rich magmas rather than Na-rich magmas responsible for the Sierra complex. Veevers (2003, 2007) suggested a similar mode of tectonic control for alkaline rocks and carbonatite (ARCs) emplaced during Gondwana amalgamation. However, although strike-slip was important during the Early Paleozoic assembly of this part of Gondwana (e.g., Rapela et al., 2007), the geochronological data presented here suggests that this complex was formed some 50 Ma before the mid-Cambrian Pampean orogeny, i.e., it was pre-orogenic. In particular, the weight of the U-Pb SHRIMP data does not support the idea of melting and crystallization of the syenite magma at 525 Ma, but merely suggests slight resetting at that time. We conclude that deep continental rifting in the Neoproterozoic rather than collisional tectonics was the likely cause of the alkaline–carbonatite magmatism, in accordance with conventional thinking on carbonatite generation (e.g., Bell et al., 1999).

Paleogeographic implications

The Grenville-age basement of Maz and Espinal, along with equivalent outcrops in the nearby Sierra de Umango (Fig. 1) (Varela et al., 2003), a Grenville-age ophiolite in the Sierra de Pie de Palo (Fig. 1) (Vujovich and Kay, 1998; Vujovich et al., 2004), and the northern part of the Arequipa–Antofalla craton in Perú were probably part of a continuous mobile belt of that age along the paleo-margin of the Amazonia craton (Casquet et al., 2008). This mobile belt has been considered as the result of collision between Amazonia and southernmost Laurentia, supposedly during the amalgamation of Rodinia (Wingate et al., 1998; Loewy et al., 2003, 2004; Tohver et al., 2002, 2004; Casquet et al., 2008).

Moreover, recent paleomagnetic evidence suggests that an ocean, i.e., the Clymene Ocean, existed at ca. 550 Ma between the Amazonia craton on one side, and the Rio de la Plata, Kalahari and Australia cratons on the other (Trindade et al., 2006). Rapela et al. (2007) have provided geological, geochemical and geochronological evidence that the Western Sierras Pampeanas Grenville-age basement was probably part of a larger continental mass that embraced the Amazonia craton, the Arequipa block of SW Peru, and other minor cratons by the time the Clymene Ocean existed. Furthermore, after consumption of the Clymene Ocean, this large continental mass underwent right-lateral (present coordinates) collision with other Gondwanan cratons to the east; e.g., collision with the Rio de la Plata and Kalahari cratons triggered the short-lived Pampean–Saldanian orogeny of Argentina and South Africa in the Early Cambrian (530–515 Ma; Rapela et al., 1998b; Rapela et al., 2007) (Fig. 2).

Opening of the Clymene Ocean could not be older than ca. 570 Ma, the age of the youngest detrital zircons found in the sedimentary Puncoviscana Formation of the Eastern Sierras Pampeanas (Schwartz and Gromet, 2004; Rapela et al., 2007). This largely turbiditic sedimentary sequence of NW Argentina, was deposited along the Kalahari margin of the Clymene ocean and moved to its present position adjacent to the Rio de la Plata craton by right-lateral displacement during the Pampean collision (Schwartz and Gromet, 2004; Rapela et al., 2007). Rifting at ca. 570 Ma leading to opening of the Clymene Ocean is the most probable scenario for the intrusion of the Maz carbonatite – syenite complex.

The western suture of the Pampean block has so far not been recognized probably because of strong Famatinian metamorphic overprint and Andean faulting throughout the Sierras Pampeanas, but it should lie somewhere between the Western Sierras Pampeanas and the easternmost Sierras de Córdoba (Fig.1). The model of DARC formation of Burke et al. (2003) and Burke and Khan (2006), according to which alkaline rock – carbonatite complexes formed at continental rifted margins at an early stage of a Wilson cycle and were finally entrapped near the suture after ocean closure and continent-continent collision, seems to apply here.

Nevertheless, the Pb-loss event recorded by some syenite zircons at ca. 525 Ma support the idea that the Western Sierras Pampeanas basement was already joined to continental Gondwana to the east by Pampean times., i.e., before the supposed Ordovician arrival of the Precordillera terrane, and was therefore not exotic to it.

Reactivation of the Grenville-age basement during the Famatinian orogeny, involving regional metamorphism and fluid infiltration under amphibolite facies and ductile deformation, was responsible for the Pb-loss and overgrowths in zircons and probably also for the fabric shown by the Maz carbonatite – syenite body. The latter is suggested by the fact that annealing-recrystallization of calcite in carbonatite requires temperatures above ca. 500ºC (Griggs et al., 1960). Pampean deformation, if any is masked by Famatinian reworking.

Implications for the magma source

Low $^{87}Sr/^{86}Sr$ ratios and the very positive εNd_{570} values suggest that the carbonatite and syenite magmas were derived from a depleted mantle source. However, the two-stage Nd model ages (T_{DM}*) between 764 and 986 Ma imply that contamination with a Nd-isotope component slightly less radiogenic than model depleted mantle at 570 Ma was involved. The age of this source is likely to be Meso/Neoproterozoic and could correspond to a lower mafic continental crust strongly depleted in light REEs during granulite facies metamorphism at ca. 1.2 Ga (Casquet et al., 2006). Petrographic, field, geochemical and geochronological evidence suggests that the carbonatite and syenite magmas were coeval. Common genesis of the less evolved syenitic magma and the carbonatites is also suggested by the parallel decrease in REE content with increasing SiO_2 /carbonate ratio from carbonatite, to silico-carbonatite to melano-foid syenite (Fig. 7), observed also in other alkaline-carbonatite complexes (e.g., Villeneuve and Relf, 1998). Chemical variation in the syenite probably arose by differentiation involving apatite and zircon among other phases, in a deep magma chamber prior to emplacement.

Conclusions

The deformed sodic syenite–carbonatite complex of the Sierra de Maz is recognized as a typical ARC in the sense of Burke et al. (2003), with very high concentrations of lithophile elements such as REE, Nb. Deformation may well be due to its involvement in the early Paleozoic orogenies of the Sierras Pampeanas, but its probable emplacement age of close to 570 Ma is consistent with Neoproterozoic lithospheric-scale rifting connected with the opening of the Clymene ocean during the break-up and dispersal of an earlier supercontinent such as Rodinia. This discovery may also have economic potential.

Acknowledgments

Financial support for this work was provided by Spanish MEC grants BTE2001-1486 and CGL2005-02065/BTE, Universidad Complutense grant PR1/05-13291 and Argentine public grants (FONCYT PICT 07-10735; CONICET PIP 5719; CONICET PEI-6275). R.J.P. acknowledges a NERC Small Research Grant. We are grateful to Kevin Burke, for suggestions based on an earlier draft of this paper and to D.L. Ashwal and an anonymous referee for their helpful comments to the manuscript.

References

Ashwal, L.D., Armstrong, R.A., Roberts, R.J., Schmitz, M.D., Corfu, F., Hetherington, C.J., Buerke, K. Gerber, M., 2007. Geochronology of large zircons from nepheline-bearing gneisses as constraints on tectonic setting: an example from southern Malawi. Contrib. Mineral. Petrol., 153, 389-403.

Attoh, K., Corfu, F., Nude, P.M., 2007. U–Pb zircon age of deformed carbonatite and alkaline rocks in the Pan-African Dahomeyide suture zone, West Africa. Precambrian Res., 155, 251-260.

Bailey, D.K., 1977. Lithospheric control of continental rift magmatism. J. Geol. Soc. London, 133, 103-106.

Bailey, D.K., 1992. Episodic alkaline activity across Africa: implications for the causes of continental break-up. In: Storey, B.C., Alabaster, A. and Pankhurst, R.J. (Eds), Magmatism and causes of continental break-up. Geol. Soc. London, Special Publications, 68, 91-98.

Baldo, E., Casquet, C., Pankhurst, R.J., Galindo, C., Rapela, C.W., Fanning, C.M., Dahlquist, J., Murra, J., 2006. Neoproterozoic A-type magmatism in the Western Sierras Pampeanas (Argentina): evidence for Rodinia break-up along a proto-Iapetus rift? Terra Nova, 18, 388-394.

Banner, J.L., Hanson, G.N., Myers, W.J., 1988. Rare earth element and Nd isotopic variations in regionally extensive dolomites from the Burlington-Keokuk Formation (Mississippian); implications for REE mobility during carbonate diagenesis. J. Sedimentary Res., 58, 415-432.

Bea, F., 1996. Residence of REE, Y, Th and U in granites and crustal protoliths; implications for the chemistry of crustal melts. J. Petrology, 37, 521-552.

Bell, K., 1989. Carbonatites: genesis and evolution. Unwin Hyman, London.

Bell, K., Kjarsgaard, B.A., Simonetti, A., 1999. Carbonatites; into the twenty-first century. J. Petrology, 39, 1839-1845.

Boynton, W.V., 1984. Geochemistry of the rare earth elements: meteorites studies. In: Henderson, P. (Ed.), Rare Earth Element Geochemistry. Developments in Geochemistry, 2, Elsevier, Amsterdam, 63-114.

Burke, K., Ashwal, L.D., Webb, S., 2003. New way to map old sutures using deformed alkaline rocks and carbonatites. Geology, 31, 391-394.

Burke, K. and Khan, S., 2006. Geoinformatic approach to global nepheline syenite and carbonatite distribution: testing a Wilson cycle model. Geosphere, 2, 53-60.

Casquet, C., Rapela, C. W., Pankhurst, R.J., Galindo, C., Dahlquist , J., Baldo, E.G., Saavedra, J., Gonzalez Casado, J.M., Fanning, C.M., 2005. Grenvillian massif-type anorthosites in the Sierras Pampeanas. J. Geol. Soc. London, 162, 9-12.

Casquet, C., Pankhurst, R.J., Fanning, C.M., Baldo, E., Galindo, C., Rapela, C.W., González-Casado, J.M., Dahlquist, J.A., 2006. U–Pb SHRIMP zircon dating of Grenvillian metamorphism in Western Sierras Pampeanas (Argentina): correlation with the Arequipa Antofalla craton and constraints on the extent of the Precordillera Terrane. Gondwana Res., 9, 524-529.

Casquet, C., Pankhurst, R.J., Rapela, C., Galindo, C., Fanning, C.M., Chiaradia, M., Baldo, E., González-Casado, J.M., Dahlquist, J.A., 2008. The Maz terrane: a Mesoproterozoic domain in the western Sierras Pampeanas (Argentina) equivalent to the Arequipa-Antofalla block of southern Peru? Implications for Western Gondwana margin evolution. Gondwana Res., 13, 163-175.

Corfu, F., Hanchar, J.M., Hoskin, P.W.O., Kinny, P., 2003. Atlas of zircon textures. In: Hanchar, J.M., Hoskin, P.W.O (Eds.), Zircon. Rev. Mineral. Geochem., 53, 469-500.

Culler, R.L., Graf, J.L., 1984. Rare earth elements in igneous rocks of the continental crust: predominantly basic and ultrabasic rocks. In: Henderson, P. (Ed.), Rare Earth Element Geochemistry. Developments in Geochemistry, 2, Elsevier, Amsterdam, 237-274.

DePaolo, D.J., Linn, A.M., Schubert, G., 1991. The continental crustal age distribution: methods of determining mantle separation ages from Sm-Nd isotopic data and application to the Southwestern United States. J. Geophys. Res., B96, 2071-2088.

Frost, R.B., Barnes, C.G., Collins, W.J., Arculus, R.J., Ellis, D.J., Frost, C.D., 2001. A geochemical classification for granitic rocks. J. Petrology, 42, 2033-2048.

Galindo, C., Casquet, C., Rapela, C., Pankhurst, R.J., Baldo, E., Saavedra, J., 2004. Sr, C and O isotope geochemistry and stratigraphy of Precambrian and Lower Paleozoic carbonate sequences from the Western Sierras Pampeanas of Argentina: tectonic implications. Precambrian Res., 131, 55-71.

Griggs, D.T., Turner, F.J., Heard H.C., 1960. Deformation of rocks at 500 to 800ºC. GSA Memoir, 79, 39-105.

Loewy, S.L., Connelly, J.N., Dalziel, I.W.D., Gower, C.F., 2003. Eastern Laurentia in Rodinia: constraints from whole-rock Pb and U/Pb geochronology. Tectonophysics, 375, 169-197.

Loewy, S.L., Connelly, J.N., Dalziel, I.W.D., 2004. An orphaned basement block: the Arequipa–Antofalla Basement of the central Andean margin of South America. GSA Bulletin, 116, 171-187.

Ludwig, K.R., 1999. Isoplot /Ex Version 2.31, a geochronological toolkit for Microsoft Excel. Berkeley Geochronological Center Special Publication, 1, 2455 Ridge Road, Berkeley, Ca 94709. USA.

Ludwig, K.R., 2001. SQUID 1.02. A user´s manual. Berkeley Geochronological Center Special Publication, 2, 2455 Ridge Road, Berkeley, Ca 94709, USA.

Lucassen, F., Becchio, R., 2003. Timing of high-grade metamorphism: Early Palaeozoic U–Pb formation ages of titanite indicate long-standing high-T conditions at the western margin of Gondwana (Argentina, 26-29ºS). J. Metamorphic Geol., 21, 649-662.

McLennan, S.M., Taylor, S.R., 1979. Rare earth element mobility associated with uranium mineralisation. Nature, 282, 247-250.

Middlemost, E., 1997. Magmas, rocks and planetary development. A survey of magma/igneous rock systems. Longman, London and New York, 299 pp.

Miller, C.F., Mc Dowell, S.M., Mapes, R.W., 2003. Hot and cold granites? Implications of zircon saturation temperatures and preservation of inheritance. Geology, 31, 529–532.

Mulcahy, S.R., Roeske, S.M., McCleland, W.C., Nomade, S., Renne, P.R., 2007. Cambrian initiation of the Las Pirquitas thrust on the western Sierras Pampeanas, Argentina: Implications for the tectonic evolution of the proto-Andean margin of South America. Geology, 35, 443-446.

Nakamura, N., 1974. Determination of REE, Ba, Fe, Mg, Na and K in carbonaceous and ordinary chondrites. Geochim. Cosmochim. Acta, 38, 757-775.

Nelson, D.R., Chivas, A.R., Chappell, B.W., McCulloch, M.T., 1988. Geochemical and isotopic systematics in carbonatite and implications for the evolution of ocean-island sources. Geochim. Cosmochim. Acta, 52, 1–7.

Porcher, C.C., Fernandes, L.A.D., Vujovich, G.I., Chernicoff, C.J., 2004. Thermobarometry, Sm/Nd ages and geophysical evidence for the location of the suture zone between Cuyania and Pampia terranes. In: Vujovich, G.I., Fernandes, L.A.D., Ramos, V.A. (Eds.), Cuyania: an exotic block to Gondwana. Gondwana Res., 7, 1057-1076.

Ramos, V.A., 2004. Cuyania, an exotic block to Gondwana: Review of a historical success and the present problems. In: Vujovich, G.I., Fernandes, L.A.D., Ramos, V.A. (Eds.), Cuyania: An exotic block to Gondwana. Gondwana Res., 7, 1009-1026.

Rapela, C.W., Pankhurst, R.J., Casquet, C., Baldo, E., Saavedra, J., Galindo, C., Fanning, C.M., 1998. The Pampean orogeny of the southern proto-Andes: Cambrian continental collision in the Sierras de Córdoba. In: Pankhurst, R.J., Rapela, C.W. (Eds), The Proto-Andean Margin of Gondwana. Geol. Soc. London, Special Publications, 142, 181-217.

Rapela, C.W., Pankhurst, R.J., Casquet, C., Baldo, E., Saavedra, J., Galindo, C., 1998. Early evolution of the proto-Andean margin of South America. Geology, 26, 707-710.

Rapela C. W., Casquet, C., Baldo, E., Dahlquist, J., Pankhurst, R.J., Galindo, C., Saavedra, J., 2002. Orogénesis del Paleozoico Inferior en el margen proto-andino de Gondwana . Sierras Pampeanas Argentina). J. Iberian Geol., 27, 23-41.

Rapela, C.W., Pankhurst, R.J., Casquet, C., Fanning, C.M., Galindo, C., Baldo, E., 2005. Datación U–Pb SHRIMP de circones detríticos en para-anfibolitas neoproterozoicas de la secuencia Difunta Correa (Sierras Pampeanas Occidentales, Argentina). Geogaceta, 38, 227-230.

Rapela, C.W., Pankhurst, R.J., Casquet, C., Fanning, C.M., Baldo, E., Gonzalez-Casado, J.M., Galindo, C., Dahlquist, J.A., 2007. The Río de La Plata craton and the assembly of SW Gondwana. Earth-Sci. Rev., 83, 49-82.

Schwartz, J.J., Gromet, L.P., 2004. Provenance of Late Proterozoic - Early Cambrian basin, Sierras de Córdoba, Argentina. Precambrian Res., 129, 1-21.

Schultz, F., Lehmann, B., Tawackoli, S., Rossling, R., Belyatsky, B., Dulski, P., 2004. Carbonatite diversity in the Central Andes: The Ayopaya alkaline province, Bolivia. Contrib. Mineral. Petrol., 148, 391–408.

Thomas, W.A., 1991. The Appalachian – Ouachita rifted margin of southeastern North America. GSA Bulletin, 103, 415-431.

Thomas, W.A., Astini, R.A., 1996. The Argentine Precordillera: a traveler from the Ouachita embayment of North America Laurentia. Science, 273, 752-757.

Thomas, W.A., Astini, R.A., 2003. Ordovician accretion of the Argentine Precordillera terrane to Gondwana: a review. J. South Am. Earth Sci., 16, 67-79.

Thompson, R.N., 1982. British Tertiary volcanic province. Scottish J. Geol., 18, 49-107.

Tohver, E., van der Pluijm, B.A., Van der Voo, R., Rizzotto, G., Scandolara, J.E., 2002. Paleogeography of the Amazon craton at 1.2 Ga: early Grenville collision with the llano segment of Laurentia. Earth Planet. Sci. Lett., 199, 185-200.

Tohver, E., Bettencourt, J.S., Tosdal, R., Mezger, K., Leite, W.B., Payolla, B.L., 2004. Terrane transfer during the Grenville orogeny: tracing the Amazonian ancestry of southern Appalachian basement through Pb and Nd isotopes. Earth Planet. Sci. Lett., 228, 161-176.

Trindade, R.I.F., D´Agrella-Filho, M.S., Epof, I., Brito Neves, B.B., 2006. Paleomagnetism of Early Cambrian Itabaiana mafic dikes (NE Brazil) and the final assembly of Gondwana. Earth Planet. Sci. Lett., 244, 361-377.

Varela, R., Sato, A., Bassei, M.A.S., Siga Jr, O., 2003. Proterozoico medio y Paleozoico inferior de la Sierra de Umango, antepais andino (29º S), Argentina: edades U–Pb y caracteristicas isotópicas. Revista Geol. Chile, 30, 265-284.

Vaughan, A.P.M., Pankhurst, R.J., 2008. Tectonic overview of the West Gondwana margin. Gondwana Res., 13, 150–162.

Vaughan, A.P.M., Scarrow, J.H., 2003. K-rich mantle metasomatism control of localization and initiation of lithospheric strike-slip faulting. Terra Nova, 15, 163–169.

Veevers, J.J., 2003. Pan-African is Pan-Gondwanaland: Oblique convergence drives rotation during 650-500Ma assembly. Geology, 31, 501-504.

Veevers, J.J., 2007. Pan-Gondwanaland post-collisional extension marked by 650-500 Ma alkaline rocks and carbonatites and related detrital zircons: A review. Earth-Sci. Rev., 83, 1-47.

Villenueve, M.E., Relf, C., 1998. Tectonic setting of 2.6 Ga carbonatites in the Slave Province, NW Canada. J. Petrology, 39, 1975-1986.

Vujovich, G.I., Kay, S.M., 1998. A Laurentian? Grenville-age oceanic arc/back-arc terrane in the Sierra de Pie de Palo, Western Sierras Pampeanas, Argentina. In: Pankhurst, R.J., Rapela, C.W. (Eds.) The Proto-Andean margin of Gondwana. Geol. Soc. London, Special Publication, 142, 159-180.

Vujovich, G.I., Van Staal, C.R., Davis, W., 2004. Age constraints and the tectonic evolution and provenance of the Pie de Palo Complex, Cuyania composite terrane, and the Famatinian orogeny in the Sierra de Pie de Palo, San Juán, Argentina. Gondwana Res., 7, 1041-1056.

Watson, E.B., 1979. Zircon saturation in felsic liquids: experimental results and applications to trace element geochemistry. Contrib. Mineral. Petrol., 70, 407–419.

Watson, E.B., Harrison, T.M., 1983. Zircon saturation revisited: Temperature and composition effects in a variety of crustal magma types. Earth Planet. Sci. Lett., 64, 295–304.

Williams, I.S., 1998. U-Th-Pb geochronology by ion microprobe. In: McKibben, M.A., Shanks, W.C. III, Ridley, W.I. (Eds.), Applications of microanalytical techniques to understanding mineralizing processes. Rev. Econ. Geol., 7, 1-35.

Wingate, M.T.D., Campbell, I.H., Compston, W., Gibson, G.M., 1998. Ion microprobe U–Pb ages for Neoproterozoic-basaltic magmatism in south-central Australia and implications for the breakup of Rodinia. Precambrian Res., 87, 135-159.

Figure captions

Figure 1. (a) Sketch map of the Sierras Pampeanas (light grey) and the Argentine Precordillera (PRE) (dark grey). (A) Ancasti, (Ch) Chepes, (Co) Córdoba, (F) Famatina, (PP) Pié de Palo, (SL) San Luís, (UME), Umango, Maz and Espinal, (V) Velasco. Mobile belts where either Grenville-age (1.0 – 1.2 Ga), Pampean (540 – 520 Ma) or Famatinian (490 – 435 Ma) deformation and metamorphism predominate are distinguished. (b) Geological sketch map of the Sierra del Maz and surrounding areas based on Casquet et al., (2006). The box indicates the location of the study area.

Figure 2. Geological map of NE Sierra de Maz based on fieldwork and interpretation of satellite raster images.

Figure 3. (a) South-facing view of the carbonatite – syenite body at its contact with the host Grenville-age gneisses and amphibolites. A screen of gneisses is visible in the centre of the

image, view width ca. 100 m. (b) Rounded coarse-grained syenite enclave wrapped in a weak foliated carbonatite matrix. (c) Very poorly-sorted and weakly-foliated breccia. Clasts consist of syenite and gneiss. The large gneiss clast is discordant to the carbonatite foliation which is parallel to the knife. (d) Carbonatite breccia. Unorientated, moderately-sorted, rounded syenite clasts in carbonatite matrix. (e) Two-stage breccia. Poorly-sorted syenite breccia (angular clasts), sharply bounded by a well-sorted weakly foliated microbreccia. Matrix is carbonatite in both facies. (f) Coarse-grained syenite with large euhedral zircon crystals.

Figure 4. (a) Nomenclature of plutonic rocks and different suite lineages, after Middlemost (1997). (b) FeOt/(FeOt + MgO) *vs.* SiO_2 wt. %, showing the Frost et al., (2001) boundary between ferroan and magnesian plutonic rocks, as well as the field of A-type granites. (c) Plot of $Na_2O + K_2O – CaO$ against SiO_2 wt. % for the syenitic suite of Sierra de Maz. Limits for the rock series and field of A-type granites are from Frost et al., (2001).

Figure 5. Plot of Zr *vs.* $N_{a2}O + K_2O/Al_2O_3$ (mol) for the syenitic suite of Sierra de Maz.

Figure 6. Eu/Eu*, P_2O_5, Sr and Y *vs.* SiO_2 wt. % for the syenitic suite of Sierra de Maz.

Figure 7. (a) Chondrite-normalized REE abundances of the syenitic suite of the Sierra de Maz complex. (b) Selected REE patterns of apatite, zircon and plagioclase from alkaline rocks and U-rich granites, from Bea (1996). Note that a modelled REE pattern for a rock with 1.9% of normative apatite closely resembles the pattern of the least evolved member of the syenitic suite (sample MAZ-12110). (c) REE, Sr and Zr plot of two silico-carbonatite samples from the Sierra de Maz complex. The open circle represents a single homogeneous crystal of carbonate separated from the carbonatite. The general carbonatite field is taken from13

samples reported by Nelson et al., (1988), whereas open squares are carbonatites reported by Villeneuve and Relf (1998). Data are normalized to chondritic values of Nakamura (1974); other normalizing data from Boynton (1984) for Tb, Ho, Tm, and Sr and Thompson (1982) for Zr.

Figure 8. Rb-Sr isochron plot of whole-rock samples from the Maz carbonatite and syenite complex

Figure 9. (a) back-scattered electron image of zircon in thin-section of syenite sample MAZ-12085, showing complex internal structure of a euhedral grain. NB in the latter image the dark areas are those relatively depleted in U and REE, whereas in the CL images such composition result in high luminescence. (b) cathodo-luminescence (CL) image of part of the analysed zircon megacryst from the Sierra de Maz syenite, showing the complex internal structure and the U–Pb ages determined from SHRIMP analyses. (c) CL image of typical fragmented crystals of zircon separated from syenite sample MAZ-12057, together with the U–Pb ages obtained from SHRIMP analyses.

Figure 10. (a) Tera-Wasserburg plot of U–Pb SHRIMP data for the zircon megacryst extracted from the syenite (Fig. 9b), error ellipses are 95% confidence limits; (b) Probability density plot (Ludwig 1999) of ^{207}Pb-corrected ^{206}Pb–^{238}U ages. Shading reflects groupings identified in the text.

Figure 11. (a) Tera-Wasserburg plot of U–Pb SHRIMP data for separated zircon from MAZ-12057 (Fig. 9c), error ellipses are 95% confidence limits; (b) Probability density plot (Ludwig 1999) of ^{207}Pb-corrected ^{206}Pb–^{238}U ages. Shading reflects groupings identified in the text.

Figure 12. a) The Clymene ocean separated a large continental mass that embraced Amazonía (AM), the Western Sierras Pampeanas (WSP), and the Arequipa-Antofalla craton (AAC) among others, from eastern Gondwana cratons (KC: Kalahari craton; RPC: Rio de la Plata craton). The Maz syenite – carbonatite body was intruded at ca. 570 Ma at the southern tip of this continental mass. Emplacement took place during early continental rifting that eventually led to opening of the Clymene Ocean. The Puncoviscana Formation was deposited on the eastern side of the Clymene Ocean (present coordinates), b) Oblique right-lateral collision produced the Pampean orogeny between 540 and 520 Ma. Paleogeographic model according to Rapela et al. (2007).

A deformed alkaline igneous rock – carbonatite complex from the Western Sierras Pampeanas, Argentina: evidence for late Neoproterozoic opening of the Clymene Ocean?

C. Casquet[a*], R.J. Pankhurst[b], C. Galindo[a], C. Rapela[c], C.M. Fanning[d],

E. Baldo[e], J. Dahlquist[e], J.M. González Casado[f†] F. Colombo[e]

[a] Dpto. Petrología y Geoquímica, Fac.Ciencias Geológicas, Inst. Geología Económica. (CSIC, Universidad Complutense), 28040 Madrid, Spain

[b] British Geological Survey, Keyworth, Nottingham NG12 5GG, UK

[c] Centro de Investigaciones Geológicas, Universidad de La Plata, 1900, La Plata, Argentina.

[d] Research School of Earth Sciences, The Australian National University, Canberra, ACT 200, Australia.

[e] CICTERRA (Conicet-Universidad Nacional de Córdoba), Vélez Sarfield 1611, 5016 Córdoba, Argentina.

[f] Dpto. de Geología y Geoquímica, Universidad Autónoma, 28049 Madrid, Spain.

† deceased

- *Corresponding author. Tel. +34 913944908; fax: +34 91
- E-mail address: casquet@geo.ucm.es

Abstract

A deformed ca. 570 Ma syenite–carbonatite body is reported from a Grenville-age (1.0 - 1.2 Ga) terrane in the Sierra de Maz, one of the Western Sierras Pampeanas of Argentina. This is the first recognition of such a rock assemblage in the basement of the Central Andes. The two main lithologies are coarse-grained syenite (often nepheline-bearing) and enclave-rich fine-grained foliated biotite-calcite carbonatite. Samples of carbonatite and syenite yield an imprecise whole rock Rb–Sr isochron age of 582 ± 60 Ma (MSWD = 1.8; Sri = 0.7029); SHRIMP U–Pb spot analysis of syenite zircons shows a total range of ^{206}Pb–^{238}U ages between 433 and 612 Ma, with a prominent peak at 560–580 Ma defined by homogeneous zircon areas. Textural interpretation of the zircon data, combined with the constraint of the Rb–Sr data suggest that the carbonatite complex formed at ca. 570 Ma. Further disturbance of the U-Pb system took place at 525 ± 7 Ma (Pampean orogeny) and at ca. 430 – 440 Ma (Famatinian orogeny) and it is concluded that the Western Sierras Pampeanas basement was joined to Gondwana during both events. Highly unradiogenic $^{87}Sr/^{86}Sr$ values in calcites (0.70275 – 0.70305) provide a close estimate for the initial Sr isotope composition of the carbonatite magma. Sm–Nd data yield εNd_{570} values of +3.3 to +4.8. The complex was probably formed during early opening of the Clymene Ocean from depleted mantle with a component from Meso-/Neoproterozoic lower continental crust.

Deleted: -

Keywords: DARCs; Syenite; U-Pb SHRIMP zircon dating; Gondwana, Rodinia.

Introduction

The association of alkaline igneous rocks (particularly nepheline syenites) with carbonatites is common in continental rift settings (Bailey, 1977, 1992; Bell, 1989; Burke et al., 2003), where they are sometimes referred to by the acronym ARCs (Alkaline Rock – Carbonatite complexes). Deformed, i.e., variably foliated concordant lenses are a special case, in which they apparently match ancient sutures in basement regions (Burke et al., 2003). Since sutures are indicative of orogenic continental collision at the end of a Wilson cycle, one interpretation of these deformed rock associations is that they represent earlier rift-related ARC assemblages that eventually became involved in the collision zone (Burke and Khan, 2006). An alternative interpretation, based on geochronological constraints, is that they formed during syn-orogenic extension related to continental orogeny, e.g., along the Dahomeyide suture zone of western Africa (Attoh et al., 2007). In a recent synthesis of the many 650–500 Ma alkaline rocks and carbonatites related to the amalgamation of Gondwana, Veevers (2003, 2007) favoured the location of these and other alkaline associations at releasing bends along transcurrent faults driven by collisional oblique stresses and during post-collisional relaxation. Vaughan and Scarrow (2003) outlined a model for the generation of potassic mafic and ultramafic magmas by transtension of metasomatized mantle.

Deleted: Moreover,

Deleted: i

We describe here the case of a Neoproterozoic deformed syenite – carbonatite body intruded into a Grenville-age (1.0 – 1.2 Ga) terrane in the Sierra de Maz, one of the Western Sierras Pampeanas of Argentina. After Rodinia break-up this terrane was involved in an Early Paleozoic collision, the Pampean orogeny, a stage in the amalgamation of SW Gondwana that involved subduction-related granite magmatism and high-grade metamorphism, largely to the east of the Western Sierras Pampeanas (Rapela et al., 2007). It is thus is a good test case for geotectonic models for deformed ARC formation. Moreover, to our knowledge this is the first recognition of such a rock assemblage of Precambrian age in the basement of the Central

Andes, which could prove to be of economic importance. Carbonatite and a diversity of alkaline silicate rocks and related hydrothermal alteration products of Cretaceous age are however well known from elsewhere in the Central Andes and its eastern foreland (e.g., Schultz et al., 2004, and references therein). Geochronological constraints and isotope geochemistry suggest that the first mode of deformed ARC formation above, i.e. early during the Pampean Wilson cycle in the late Neoproterozoic, probably applies in the case of the Maz syenite – carbonatite body. Moreover syenite and carbonatite magmas were coeval and were mainly fed from a depleted mantle source, probably with a minor contribution from a poorly radiogenic continental crust of Grenville age.

Geological and paleogeographical setting

The Sierras Pampeanas of Argentina are elongated blocks of pre-Andean crystalline basement that were exposed to erosion by tilting during Cenozoic Andean tectonics (Fig. 1). Three metamorphic and igneous belts have been distinguished (for a review, see Rapela et al., 1998a, 2002). (1) The older is of 'Grenville' age, ca. 1.0 to 1.2 Ga, and crops out in the Western Sierras Pampeanas. (2) The Pampean belt is of Early Cambrian age, between 530 and 515 Ma, and crops out in the Eastern Sierras Pampeanas. (3) The Famatinian belt of Ordovician age, ca. 490 to 430 Ma, is located between the former two and is the best preserved. Famatinian metamorphism, deformation and magmatism overprint with varied extent and intensity the Grenvillian and Pampean belts. The Sierra de Maz is one of the Western Sierras Pampeanas where Grenville-age metamorphic and igneous rocks have been recognized (Porcher et al., 2004; Casquet et al., 2005, 2006, 2008). Other larger outcrops of Grenville-age rocks exist in the Sierra de Pie de Palo (see review by Ramos, 2004) and Umango (Varela et al., 2003) (Fig. 1).

Paleogeographic reconstructions and dynamic interpretations of the proto-Andean margin of Gondwana in the Mesoproterozoic to Ordovician time span have been strongly stimulated over the past fifteen years by the hypothesis of allochthoneity of the Precordillera terrane (e.g., Vaughan and Pankhurst, 2008). According to most supporters of the hypothesis, this terrane consists of a Grenville-age basement that crops out in the Western Sierras Pampeanas and a non-metamorphic Early Cambrian to Middle Ordovician passive margin cover sequence, i.e., the Argentine Precordillera (Fig. 1) (for reviews see Thomas and Astini, 2003; Ramos, 2004). In this paradigm, the Precordillera terrane is an exotic terrane rifted away from the Ouachita embayment in the Appalachian margin of eastern Laurentia in the Early Cambrian that collided with the proto-Andean margin of Gondwana in the Ordovician to produce the Famatinian orogeny (Thomas, 1991; Thomas and Astini, 1996). However, whether the Grenvillian outcrops in Western Sierras Pampeanas are part of the exotic terrane or not has also been questioned (Galindo et al., 2004; Rapela et al., 2005; Casquet et al., 2008). In a recent contribution Rapela et al. (2007) suggested that after initial break-up of Rodinia the Western Sierras Pampeanas Grenville-age basement was part of a larger continental mass embracing the Mesoproterozoic central and northern Arequipa–Antofalla craton (Peru), and the Amazonia craton (Brazil). These continental domains coalesced during the Sunsas (Grenville-age) orogeny (Loewy et al., 2004; Tohver et al., 2002, 2004; Casquet et al., 2008). This large continent collided obliquely with the Rio de la Plata and Kalahari cratons to the east (present coordinates) to produce the Pampean orogeny in the early Cambrian, with the disappearance of the intervening Clymene Ocean (Trindade et al., 2006).

Field description

The Maz deformed syenite–carbonatite complex forms a body ca. 4 km long and of variable thickness (max. 120 m), striking 340–345º along the eastern margin of the Sierra de

Maz and dipping 65–70º E. (Figs 2, 3a). Host rocks are: 1) hornblende-biotite-garnet gneisses and biotite-garnet gneisses with some interleaved quartzites and marbles, 2) ortho-amphibolites, metagabbros and local meta-peridotites; 3) massif-type anorthosites of 1070 ± 41 Ma (Casquet et al., 2005) and a variety of coeval granitic orthogneisses. Host rocks to the complex (Fig. 1b) belong to the Maz Central Domain (Casquet et al., 2008), which underwent granulite facies metamorphism at ca. 1.2 Ga and retrogression under amphibolite facies conditions at 431 ± 40 Ma (Casquet et al., 2006, 2008). The intrusion is largely concordant, but locally discordant, to the foliation of the host rocks (Fig. 2).

Homogeneous medium- to coarse-grained syenite and fine-grained foliated biotite carbonatite are the two main lithologies forming the body. They do not show a clear internal arrangement, syenite ranging from elongated bodies tens of metres long down to few centimetre-size spheroidal enclaves in the carbonatite. Carbonatite foliation wraps around the syenite bodies that are locally foliated as well (Fig. 3b). Besides syenite, the carbonatite hosts a number of other types of enclaves, notably large (up to several centimetres) isolated crystals of albite and biotite, coarse-grained mafic enclaves, and enclaves of the host gneisses and amphibolites with the internal foliation in places at a high angle to the carbonatite foliation (Fig. 3c). Enclaves are rounded to sub-angular and vary from well- to poorly-sorted in terms of size from place to place, and can be locally very abundant, giving the outcrop a breccia-like aspect (Fig. 3d). Enclaves of an earlier carbonatite (also with enclaves) can be found within a younger carbonatite. Variability in the number and sorting of the enclaves suggests that their incorporation in the carbonatite magma was a multi-stage process (Fig. 3e). The syenites contain visible pinkish zircon megacrysts that can attain few cm size (Fig. 3f), a feature also recognized in carbonatite – syenite bodies elsewhere (Ashwal et al., 2007). Coarse-grained calcite veins and interstitial calcite are locally found in syenites.

Petrography and mineralogy

The carbonatite consists of calcite, 10 to 30 % modal biotite, abundant anomalous biaxial apatite, and minor magnetite, zircon, very scattered U-rich pyrochlore, and columbite. Compositionally the calcite has up to 1.3 wt. % SrO, 2.5 wt. % FeO, and 0.41 wt. % ΣLREE (Table 1 and microprobe data not included here). Electron microprobe analyses of the biotite show an average Fe# value [Fe/(Mg+Fe)] of 0.74 and Al^{IV} = 2.643–2.748 a.f.u.; the apatite has up to 2.76 wt. % F, the pyrochlore 18.60–30.23 wt. % UO_2 and the columbite Nb/Nb+Ta = 0.98. Calcite crystals are fine-grained granoblastic with a slight preferred orientation and narrow straight twins. Lattice-preferred orientation is weak but relics of larger strained crystals of calcite are preserved within the foliated granoblastic groundmass, suggesting that the latter probably arose by recrystallization of former coarser-grained, probably primary, carbonate crystals. Groundmass biotite is found as individual plates but more commonly as fine-grained recrystallized aggregates, often as rims on isolated rounded albite crystals or larger albite syenite spheroids. The visible foliation largely results from preferred orientation of biotite.

The syenites are coarse-grained rocks that are locally foliated. They consist of albite ($Ab_{95.0\text{-}97.5}An_{2.2\text{-}2.6}Or_{0.9\text{-}2.5}$) and biotite chemically similar to that in the carbonatite (Fe# = 0.83). Subordinate microcline is found at albite grain boundaries, as either replacement or exolution. Undulose extinction and deformation bands in albite, and bending and kinking in biotite, are common in non-foliated varieties. K-rich nepheline ($Ks_{21\text{-}22}$), variably converted to a fine-grained micaceous aggregate, was found in several samples. Accessory minerals are zircon, anomalous biaxial apatite and minor pyrochlore. Secondary minerals in the syenites are calcite, muscovite-sericite after K-feldspar and chlorite and epidote after biotite. Syenite spheroids within the carbonatite consist of an inner coarse-grained core and a continuous fine-grained mantle resembling a chilled margin, rimmed by fine-grained biotite. Foliated syenites

Deleted: s

Deleted: s

are medium-grained and show a granoblastic orientation of albite and preferred orientation of biotite.

Besides large biotite and albite megacrysts, two types of mafic enclaves have been found in the carbonatite. One type consists of coarse-grained aegirine-augite (Na_2O = 5.35–5.75 wt. %) variably converted to katophorite amphibole, albite, Fe-rich calcite and magnetite. The second type consists of coarse-grained magnetite and biotite with accessory primary calcite (included in biotite), apatite and pyrochlore.

Analytical procedures

Full chemical analyses of four syenite and two carbonatite samples were performed at ACTLABS (Canada): major oxides by ICP and trace elements by ICP-MS. Other determinations at ACTLABS were Cl (INAA), CO_2 (COUL), F (FUS-ISE), and S (IR). Fe^{2+} was determined volumetrically at the Centro de Investigaciones Geológicas, La Plata. Major and trace elements of one probably relic calcite megacryst were determined by XRF (Table 1) and mineral compositions by electron microprobe at the Universidad Complutense, Madrid (Supplementary Table obtainable from the Precambrian Research Data Repository) .

Rb–Sr systematics were analysed in three samples of carbonatite, four of syenite, two vein calcites in syenites, and four enclaves in carbonatite – an aegirine mafic enclave (see below) and three megacrysts, two of biotite and one of albite. For Sm–Nd systematics five samples were analysed: two syenites and three carbonatites. Samples were crushed and powdered to ~ 200 mesh. For the carbonatite samples, Sr and Nd isotope composition was obtained by leaching 200 mg of each sample in10 ml of acetic acid for 12 hours. Whole-rock syenites and silicate minerals were first decomposed in 4 ml HF and 2 ml HNO_3, in Teflon digestion bombs during 48 hours at 120 ºC and finally in 6M HCl. Elemental Rb, Sr, Sm and Nd in carbonates and silicates were determined by isotope dilution using spikes enriched in ^{87}Rb,

^{84}Sr, ^{149}Sm and ^{150}Nd. Ion exchange techniques were used to separate the elements for isotopic analysis. Rb, Sr and REE were separated using Bio-Rad AG50 x 12 cation exchange resin. Sm and Nd were further separated from the REE group using Bio-beads coated with 10% HDEHP. All isotopic analyses were carried out on a VG Sector 54 multicollector mass spectrometer at the Geocronología y Geoquímica Isotópica Laboratory, Complutense University, Madrid, Spain. Isotope data are shown in Table 2. Errors in the initial ratios are reported at 2σ.

U-Th-Pb analyses were performed on two samples using SHRIMP II at the Research School of Earth Sciences, The Australian National University, Canberra. One was a euhedral zircon megacryst up to 1.5 cm in width, extracted from a syenite; the second was a hand-picked concentrate separated after milling another syenite. Zircon fragments were mounted in epoxy together with chips of the Temora reference zircon , ground approximately half-way through and polished. Reflected and transmitted light photomicrographs, and cathodo-luminescence (CL) SEM images, were used to decipher the internal structures of the sectioned grains and to target specific areas within the zircons. Each analysis consisted of 6 scans through the mass range. The data were reduced in a manner similar to that described by Williams (1998, and references therein), using the SQUID Excel Macro of Ludwig (2001). Data for the geochronology samples are given in Table 3.

Geochemistry

Major and trace elements

The syenitic rocks display a relatively wide, alkali-rich compositional range from nepheline monzosyenites (52% SiO_2) to normal syenites (58–64% SiO_2) (Table 1, Fig. 4), and are Na-rich (K_2O/Na_2O mol ≤ 0.33). They plot in the alkali and ferroan fields of the Frost et al. (2001) diagram, clearly indicating an alkaline signature for the parental magma (Figs 4b, 4c).

The Zr content of the suite is remarkably high (716–1920 ppm), consistent with experimental evidence indicating that Zr is more soluble in peralkaline than in metaluminous melts (Watson, 1979; Watson and Harrison, 1983). A negative correlation between Zr and Agpaitic Index (Fig. 5a) strongly suggests that the alkali content of the melt controlled the crystallization of zircon. Zircon saturation temperatures (T_{Zr}) calculated from bulk-rock compositions using the equations of Watson and Harrison (1983) and Miller et al. (2003), yield initial temperatures of crystallization between 826ºC and 1022ºC, similar to those recorded for basaltic magmas.

The syenitic suite shows a strong decrease in P_2O_5, REE_{total}, Sr and Y with SiO_2 (Fig. 6). REE patterns also change significantly with silica content, from $[La/Yb]_N = 26$ in the least evolved rock, to a U-shaped pattern with $[La/Yb]_N = 2.33$ and a well-developed positive Eu anomaly in the most evolved one (Fig. 7a). P_2O_5 contents decrease from 0.74% (1.9% normative apatite) in the least evolved syenite to 0.02% (0.05% normative apatite) in the most evolved one.

The REE pattern of the nepheline monzosyenite (MAZ-12110, Fig. 7a) might reasonably suggest control entirely by the modal content of apatite (Fig. 7b). However, the HREE distribution cannot be explained by fractionation of apatite alone, particularly in the rocks of intermediate composition, as the decreasing slope of the patterns suggests crystallization of a mineral phase with a high partition coefficient for HREE, such as zircon (Fig. 7a and b). As noted above, zircon is a conspicuous accessory mineral in the syenitic suite, with megacrysts up to a few cm in size. Coupled fractionation of apatite and zircon may replicate the observed REE patterns in the syenites of intermediate composition (SiO_2 = 58–61 %). The depletion of REE in the most evolved syenites (SiO_2 = 64%) may be explained by the effective fractionation of accessory minerals, leaving plagioclase-rich residual liquids (Fig. 7a and b).

The two carbonatite samples (Table 1) are silico-carbonatites that have steep, LREE-enriched patterns with no Eu anomalies, and plot within the field defined for most world-wide carbonatites (Fig. 7c). They also contain large amounts of Ti, Nb, Y, Sr and Ba (Table 1), as usually reported in carbonatite complexes (e.g., Culler and Graf, 1984). Compared with the carbonatite whole-rock REE patterns, the REE analysis by XRF of a relic large homogeneous crystal of calcite (Table 1, sample MAZ-12090), shows a parallel but slightly more enriched pattern (Fig. 7c). The REE pattern of the least evolved member of the syenitic suite (MAZ-12110) (Fig. 7a), has lower total REE content than associated carbonatites, but similar LREE/HREE ratios (Fig. 7c), a characteristic that has been reported in several alkaline-carbonatite complexes (e.g., Culler and Graf, 1984; Villenueve and Relf, 1998).

Rb–Sr and Sm–Nd Isotope Systematics

The present-day Sr isotope compositions of the carbonatite calcite and vein calcite are similar and very unradiogenic (Table 2). The slightly higher $^{87}Sr/^{86}Sr$ values in the carbonatite calcite (0.70299–0.70305) than in vein calcite (0.70275–0.70277) is probably due to very minor contamination of the carbonatite leachate with Sr derived from biotite. In all cases the very low $^{87}Rb/^{86}Sr$ ratios of the calcites resulting from the very high Sr contents (3108–8493 ppm), mean that the Sr isotope composition is almost invariant with age (Table 2) and the present values can thus be taken as a close estimate for the initial Sr isotope composition of the carbonatite magma at the time of formation, i.e., 0.7027 to 0.7030. When carbonatites and syenite data are plotted as $^{87}Rb/^{86}Sr$ *vs.* $^{87}Sr/^{86}Sr$, an isochron age of 582 ± 60 Ma (MSWD = 1.8; Sr_i = 0.7029) is obtained (Fig. 8). For this plot only syenites MAZ-12057 and MAZ-12085 were used because they do not show evidence of significant alteration of primary minerals (syenites MAZ-12058 and MAZ 12110 show deformation and strong alteration of nepheline and biotite). The albite megacryst and the aegirine mafic enclave both have high Sr

Deleted: for

contents (4211 and 3108 ppm, respectively) and low $^{87}Rb/^{86}Sr$ ratios (Table 2). When these data are included in the isochron dataset an indistinguishable age is obtained (565 ± 60 Ma, MSWD = 3.3, Sr_i = 0.70300). The two biotite megacrysts have model ages (assuming an initial $^{87}Sr/^{86}Sr$ of 0.703, of 490 ± 7 and 480 ± 11 Ma, indicating either late crystallization (or loss of radiogenic Sr) – see below. The very unradiogenic nature of the carbonate Sr isotope composition suggests a significant contribution to the magma from a depleted source.

Sm–Nd data (Table 2) yield epsilon values at the reference age of 570 Ma (εNd_{570}) between +3.3 and +4.8, also suggesting a major contribution to the Nd isotope composition of magma from a depleted mantle source. Nd model ages (T_{DM}*) between 764 and 986 Ma are significantly older than those obtained from the Rb–Sr data and zircon chronology (see below). The Sm–Nd data for the five analysed whole-rock do not fit an isochron (MSWD 10.2), suggesting that Sm-Nd systematics were perturbed after magmatic crystallization; chemical and geochronological evidence from zircon is consistent with this interpretation.

Zircon internal structure and U–Pb chronology

A feature of the syenite is the presence of euhedral mm-size pinkish zircon crystals, which has also been found in nepheline-syenite carbonatite complexes elsewhere (Ashwal et al., 2007). Megacrysts up to a few cm in size are also randomly distributed (Fig. 3f). Internal fractures are common. Back-scattered electron (BSE) images (Fig. 9a) show a complex zoning pattern probably resulting from post-crystallization modification. Light-coloured zones are enriched in Th, U and REE and are poorer in Hf compared to the darker ones.

Zircon megacryst,

One megacryst (MAZ-12089) was extracted in the field for initial study. Cathodo-luminescence (CL) images (Fig. 9b) show that it has a very complex internal structure. The oldest zircon in textural terms appears as internal areas of relatively uniform growth with low luminescence; there are also areas of higher luminescence and rather irregular alternating structure which are nevertheless relatively homogeneous. However, large irregular areas have variable luminescence with complex internal structure which appears to be secondary. Within the latter we distinguish areas of complex patchy texture, and areas in which highly luminescent microveins penetrate the old homogeneous zones, apparently resulting from replacement or recrystallization along cracks. Such complex textures are usually ascribed to late or post-magmatic processes, including hydrothermal alteration, and metamorphism (see Corfu et al., 2003, figures 6-16, 10-5 and 11-7). Finally, there is one peripheral area with more regular oscillatory zoning that could represent newer growth.

SHRIMP U–Pb spot analysis (Table 3a) shows that the structural complexity corresponds to a large extent with variable isotope systematics. The total range of apparent ^{206}Pb-^{238}U ages is 433–612 Ma, but most of the areas in relatively homogeneous domains yield ages of 530–590 Ma (e.g., Fig. 9b), with a single anomalous age of 612 Ma, whereas the mosaic areas generally yielded ages of <500 Ma. The outer oscillatory-zoned domain also yielded younger ages of 450–495 Ma (spots 1, 2, 3), clearly reflecting much later re-growth. Overall, there is no obvious correlation between age and either U content or Th/U ratio. Eight results from the most homogeneous areas (spots 5,6, 10, 12, 14, 14 and 16 in Table 3) gave a weighted mean age of 566 ± 8 Ma (MSWD 1.5) and three within the more complex areas (spots 9, 11 and 18) gave 530 ± 19 Ma (MSWD 1.4). These results are illustrated in a Tera-Wasserburg plot and a probability density diagram (Fig. 10a and 10b, respectively).

Groundmass Zircon

Zircon extracted from whole-rock crushing of syenite MAZ-12057 consists entirely of irregularly-shaped grains up to 500 μm in length of clear but heavily fractured zircon. The internal structure revealed by CL predominantly corresponds to the more homogenous type seen in the megacryst, albeit still with irregular cross-cutting zones with alternating structure (Fig. 9c). The absence of euhedral grains and the incomplete internal structures indicate that these grains are not individual crystals but fragments of larger grains, broken along internal fractures either in a geological event or during the mineral separation process. The latter is suggested by the occasional occurrence of mosaic patterned grains and is confirmed by examination of *in situ* zircon crystals in petrographic thin sections of other samples of the syenite (e.g., Fig. 9a) which show more complete zoned domains but extensive fractures.

The ^{206}Pb-^{238}U ages obtained from the fragmented grains of MAZ-12057 (Table 3b) are similar to those from the more homogeneous domains of the megacryst, ranging from 495 to 588 Ma (see Fig 11a, b). Even this more limited range is well outside the analytical uncertainty of the individual results and encompasses a distribution that is at least bi-modal, twenty-two of the ages clustering around a broad peak at 571 ± 5 Ma (albeit with MSWD =2.8) and a smaller group of five defining a weighted mean of 525 ± 7 Ma (MSWD = 0.2) and a single age at 495 Ma. As with the megacryst analyses there is no obvious relationship between age and parameters such as U content or Th/U ratio.

Discussion

The Maz outcrop is an example of a *deformed alkaline rock – carbonatite* complex. This is the first such complex to be described from the crystalline basement of the Andes. Beyond its potential economic importance (Nb, REE), this type of complex can be of value in constraining geodynamic and paleogeographic models of continental dispersal and amalgamation if the age of intrusion is defined.

Chronological interpretation and geodynamic implications

The Maz carbonatite – syenite was intruded into a Grenville-age basement that forms the central and eastern side of the sierra. The local obliquity of the body to the regional foliation and the fact that rotated blocks of the host gneisses are locally found in the carbonatite, together with the zircon U-Pb geochronological data presented here, show that its emplacement age is post-Grenvillian. In the absence of any textural indication of inheritance, it is most probable that the older zircon ages, yielding means of 566 ± 7 Ma in the case of the megacryst and 571 ± 5 Ma in that of the groundmass zircon, represent igneous crystallization during the Late Neoproterozoic. It is difficult to know whether the spread of the latter group indicated by the MSWD of 2.8 might signify more than one event; the most definitive statement that can be made concerning the age of this carbonatite complex is that it was emplaced within the interval 565–580 Ma, most probably at ca. 570 Ma, i.e., Ediacaran.

The Rb–Sr whole rock systematics reinforce this interpretation; the two calculated isochron ages (582 ± 60 Ma and 565 ± 60 Ma) are within error of the U–Pb zircon ages. The large uncertainties in these ages are due to the limited range of Rb/Sr ratios, and this might lead to some doubts over the confidence of this result. However, we note that the whole-rock Rb-Sr system in these rocks appears to have been resistant to disturbance during the amphibolite-facies Famatinian metamorphism and deformation at ca. 430–440 Ma, which affected the whole region (Lucassen and Becchio, 2003; Casquet et al., 2005, 2008). A significantly older maximum possible age for the carbonatite – syenite complex might be suggested by the Sm-Nd T_{DM}* model ages of 764–986 Ma, but in view of the fact that the whole-rock syenites do not yield a reasonable Sm-Nd isochron, these seem as likely to reflect metamorphic disturbance of the Sm–Nd systems in a carbonate-rich environment, where REE are known to be relatively mobile (McLennan and Taylor, 1979; Banner et al., 1988). Alternatively, pre-crystallization Sm-Nd systematics may reflect some crustal contribution to the magma.

Deleted: T

Deleted: was

Deleted: is supported by the fact that it was not reset

Deleted: Ma

Deleted: that

Consequently we conclude that the Maz carbonatite – syenite complex is the first evidence of a Late Neoproterozoic rifting event in the Western Sierras Pampeanas.

In the case of the zircon megacryst it would be possible to interpret the few ages at ~520 Ma as due to partial Pb-loss. On the other hand, the well-defined age grouping at 525 ± 7 Ma given by zoned zircon in the whole-rock syenite, where Famatinian reworking is clearly minor (only one age of <500 Ma), seems to indicate a specific event related to rejuvenation at the time of the Pampean orogeny (Rapela et al., 1998b). The zoned zircon areas that yield this age are not texturally distinguishable from the older zircon (there is certainly no evidence for any core–rim relationship indicating re-growth), implying that these Pampean ages represent cryptic Pb-loss in a discrete event.

This interpretation of the ~525 Ma U-Pb zircon ages may be taken as further evidence of the effects of the Early Cambrian Pampean orogeny in the Western Sierras Pampeanas. Until now most reliable metamorphic ages in the Maz and Espinal area were either Grenville-age (ca. 1.2 Ga) or Famatinian (430–440 Ma, e.g., Lucassen and Becchio, 2003; Porcher et al., 2004; Casquet et al., 2005, 2006, 2008; and our unpublished data). Involvement of the Western Sierras Pampeanas Grenville-age basement in the Pampean orogeny has, however, been recently emphasized by Rapela et al. (2007). Recent determinations of a single U–Pb titanite age of ca. 530 Ma from the southern tip of the Sierra de Maz (Lucassen and Becchio, 2003) and of a metamorphic hornblende Ar-Ar age of ca. 515 Ma in the Grenvillian basement of the Sierra de Pie de Palo, south of Sierra de Maz (Mulcahy et al., 2007), strengthens this geodynamic interpretation.

According to the majority of the textural evidence, the younger ages of 433–495 Ma, particularly in the megacryst, are almost certainly related to minor zircon growth and variable Pb-loss, in part caused by invasive fluids penetrating along fractures, and would correspond to reactivation during Famatinian metamorphism. The highly fractured nature of the zircon megacryst would probably also have facilitated fluid exchange processes. Evidence for deformation and metamorphic rejuvenation under amphibolite facies conditions in the Maz and Espinal area at ca. 430 - 440 Ma has been shown by Lucassen and Becchio (2003), Porcher et al. (2004) and Casquet et al. (2005, 2008).

Tectonic implications

The rock association of alkali-syenite (+ nepheline) and carbonatite, with no evidence for associated alkali basalts shows that this is not a high-thermal anomaly mantle plume scenario, but was most probably related to an extensional environment. Vaughan and Scarrow (2003) suggested transtensional tectonics in a metasomatized mantle, but this produces K-rich magmas rather than Na-rich magmas responsible for the Sierra complex. Veevers (2003, 2007) suggested a similar mode of tectonic control for alkaline rocks and carbonatite (ARCs) emplaced during Gondwana amalgamation. However, although strike-slip was important during the Early Paleozoic assembly of this part of Gondwana (e.g., Rapela et al., 2007), the geochronological data presented here suggests that this complex was formed some 50 Ma before the mid-Cambrian Pampean orogeny, i.e., it was pre-orogenic. In particular, the weight of the U-Pb SHRIMP data does not support the idea of melting and crystallization of the syenite magma at 525 Ma, but merely suggests slight resetting at that time. We conclude that deep continental rifting in the Neoproterozoic rather than collisional tectonics was the likely cause of the alkaline–carbonatite magmatism, in accordance with conventional thinking on carbonatite generation.

Paleogeographic implications

The Grenville-age basement of Maz and Espinal, along with equivalent outcrops in the nearby Sierra de Umango (Fig. 1) (Varela et al., 2003), a Grenville-age ophiolite in the Sierra de Pie de Palo (Fig. 1) (Vujovich and Kay, 1998; Vujovich et al., 2004), and the northern part of the Arequipa–Antofalla craton in Perú were probably part of a continuous mobile belt of that age along the paleo-margin of the Amazonia craton (Casquet et al., 2008). This mobile belt has been considered as the result of collision between Amazonia and southernmost Laurentia, supposedly during the amalgamation of Rodinia (Wingate et al., 1998; Loewy et al., 2003, 2004; Tohver et al., 2002, 2004; Casquet et al., 2008).

Moreover, recent paleomagnetic evidence suggests that an ocean, i.e., the Clymene Ocean, existed at ca. 550 Ma between the Amazonia craton on one side, and the Rio de la Plata, Kalahari and Australia cratons on the other (Trindade et al., 2006). Rapela et al. (2007) have provided geological, geochemical and geochronological evidence that the Western Sierras Pampeanas Grenville-age basement was probably part of a larger continental mass that embraced the Amazonia craton, the Arequipa block of SW Peru, and other minor cratons by the time the Clymene Ocean existed. Furthermore, after consumption of the Clymene Ocean, this large continental mass underwent right-lateral (present coordinates) collision with other Gondwanan cratons to the east; e.g., collision with the Rio de la Plata and Kalahari cratons triggered the short-lived Pampean–Saldanian orogeny of Argentina and South Africa in the Early Cambrian (530–515 Ma; Rapela et al., 1998b; Rapela et al., 2007) (Fig. 2).

Opening of the Clymene Ocean could not be older than ca. 570 Ma, the age of the youngest detrital zircons found in the sedimentary Puncoviscana Formation of the Eastern Sierras Pampeanas (Schwartz and Gromet, 2004; Rapela et al., 2007). This largely turbiditic sedimentary sequence of NW Argentina, was deposited along the Kalahari margin of the Clymene ocean and moved to its present position adjacent to the Rio de la Plata craton by right-lateral displacement during the Pampean collision (Schwartz and Gromet, 2004; Rapela et al., 2007). Rifting at ca. 570 Ma leading to opening of the Clymene Ocean is the most probable scenario for the intrusion of the Maz carbonatite – syenite complex.

Deleted: Perú

The western suture of the Pampean block has so far not been recognized probably because of strong Famatinian metamorphic overprint and Andean faulting throughout the Sierras Pampeanas, but it should lie somewhere between the Western Sierras Pampeanas and the easternmost Sierras de Córdoba (Fig.1). The model of DARC formation of Burke et al. (2003) and Burke and Khan (2006), according to which alkaline rock – carbonatite complexes formed at continental rifted margins at an early stage of a Wilson cycle and were finally entrapped near the suture after ocean closure and continent-continent collision, seems to apply here.

Nevertheless, the Pb-loss event recorded by some syenite zircons at ca. 525 Ma support the idea that the Western Sierras Pampeanas basement was already joined to continental Gondwana to the east by Pampean times., i.e., before the supposed Ordovician arrival of the Precordillera terrane, and was therefore not exotic to it.

Reactivation of the Grenville-age basement during the Famatinian orogeny, involving regional metamorphism and fluid infiltration under amphibolite facies and ductile deformation, was responsible for the Pb-loss in zircons and probably also for the fabric shown by the Maz carbonatite – syenite body. The latter is suggested by the fact that annealing-recrystallization of calcite in carbonatite requires temperatures above ca. 500ºC (Griggs et al., 1960).

Implications for the magma source

Low $^{87}Sr/^{86}Sr$ ratios and the very positive εNd_{570} values suggest that the carbonatite and syenite magmas were derived from a depleted mantle source. However, the two-stage Nd model ages (T_{DM}*) between 764 and 986 Ma imply that contamination with a Nd-isotope component slightly less radiogenic than model depleted mantle at 570 Ma was involved. The age of this source is likely to be Meso/Neoproterozoic and could correspond to a lower mafic continental crust strongly depleted in light REEs during granulite facies metamorphism at ca. 1.2 Ga (Casquet et al., 2006). Petrographic, field, geochemical and geochronological evidence suggests that the carbonatite and syenite magmas were coeval. Common genesis of the less evolved syenitic magma and the carbonatites is also suggested by the parallel decrease in REE content with increasing SiO_2 /carbonate ratio from carbonatite, to silico-carbonatite to melano-foid syenite (Fig. 7), observed also in other alkaline-carbonatite complexes (e.g., Villeneuve and Relf, 1998). Chemical variation in the syenite probably arose by differentiation involving apatite and zircon among other phases, in a deep magma chamber prior to emplacement.

Conclusions

Formatted: Font: Bold

The deformed sodic syenite–carbonatite complex of the Sierra de Maz is recognized as a typical ARC in the sense of Burke et al. (2003), with very high concentrations of lithophile elements such as REE, Nb. Deformation may well be due to its involvement in the mid-Cambrian Pampean orogeny of the Sierras Pampeanas, but its probable emplacement age of close to 570 Ma is consistent with Neoproterozoic lithospheric-scale rifting connected with the openinbg of the Clymene ocean during the break-up and dispersal of an earlier supercontinent such as Rodinia. This discovery may also have economic potential.

Acknowledgments

Financial support for this work was provided by Spanish MEC grants BTE2001-1486 and CGL2005-02065/BTE, Universidad Complutense grant PR1/05-13291 and Argentine public grants (FONCYT PICT 07-10735; CONICET PIP 5719; CONICET PEI-6275). R.J.P. acknowledges a NERC Small Research Grant. We are grateful to Kevin Burke, for suggestions based on an earlier draft of this paper and to D.L. Ashwal and an anonymous referee for their helpful comments to the manuscript.

References

Ashwal, L.D., Armstrong, R.A., Roberts, R.J., Schmitz, M.D., Corfu, F., Hetherington, C.J., Buerke, K. Gerber, M., 2007. Geochronology of large zircons from nepheline-bearing gneisses as constraints on tectonic setting: an example from southern Malawi. Contrib. Mineral. Petrol., 153, 389-403.

Attoh, K., Corfu, F., Nude, P.M., 2007. U–Pb zircon age of deformed carbonatite and alkaline rocks in the Pan-African Dahomeyide suture zone, West Africa. Precambrian Res., 155, 251-260.

Bailey, D.K., 1977. Lithospheric control of continental rift magmatism. J. Geol. Soc. London, 133, 103-106.

Bailey, D.K., 1992. Episodic alkaline activity across Africa: implications for the causes of continental break-up. In: Storey, B.C., Alabaster, A. and Pankhurst, R.J. (Eds), Magmatism and causes of continental break-up. Geol. Soc. London, Special Publications, 68, 91-98.

Baldo, E., Casquet, C., Pankhurst, R.J., Galindo, C., Rapela, C.W., Fanning, C.M., Dahlquist, J., Murra, J., 2006. Neoproterozoic A-type magmatism in the Western Sierras Pampeanas (Argentina): evidence for Rodinia break-up along a proto-Iapetus rift? Terra Nova, 18, 388-394.

Banner, J.L., Hanson, G.N., Myers, W.J., 1988. Rare earth element and Nd isotopic variations in regionally extensive dolomites from the Burlington-Keokuk Formation (Mississippian); implications for REE mobility during carbonate diagenesis. J. Sedimentary Res., 58, 415-432.

Bea, F., 1996. Residence of REE, Y, Th and U in granites and crustal protoliths; implications for the chemistry of crustal melts. J. Petrology, 37, 521-552.

Bell, K., 1989. Carbonatites: genesis and evolution. Unwin Hyman, London.

Boynton, W.V., 1984. Geochemistry of the rare earth elements: meteorites studies. In: Henderson, P. (Ed.), Rare Earth Element Geochemistry. Developments in Geochemistry, 2, Elsevier, Amsterdam, 63-114.

Burke, K., Ashwal, L.D., Webb, S., 2003. New way to map old sutures using deformed alkaline rocks and carbonatites. Geology, 31, 391-394.

Burke, K. and Khan, S., 2006. Geoinformatic approach to global nepheline syenite and carbonatite distribution: testing a Wilson cycle model. Geosphere, 2, 53-60.

Casquet, C., Rapela, C. W., Pankhurst, R.J., Galindo, C., Dahlquist , J., Baldo, E.G., Saavedra, J., Gonzalez Casado, J.M., Fanning, C.M., 2005. Grenvillian massif-type anorthosites in the Sierras Pampeanas. J. Geol. Soc. London, 162, 9-12.

Casquet, C., Pankhurst, R.J., Fanning, C.M., Baldo, E., Galindo, C., Rapela, C.W., González-Casado, J.M., Dahlquist, J.A., 2006. U–Pb SHRIMP zircon dating of Grenvillian metamorphism in Western Sierras Pampeanas (Argentina): correlation with the Arequipa Antofalla craton and constraints on the extent of the Precordillera Terrane. Gondwana Res., 9, 524-529.

Casquet, C., Pankhurst, R.J., Rapela, C., Galindo, C., Fanning, C.M., Chiaradia, M., Baldo, E., González-Casado, J.M., Dahlquist, J.A., 2008. The Maz terrane: a Mesoproterozoic domain in the western Sierras Pampeanas (Argentina) equivalent to the Arequipa-Antofalla block of southern Peru? Implications for Western Gondwana margin evolution. Gondwana Res., 13, 163-175.

Corfu, F., Hanchar, J.M., Hoskin, P.W.O., Kinny, P., 2003. Atlas of zircon textures. In: Hanchar, J.M., Hoskin, P.W.O (Eds.), Zircon. Rev. Mineral. Geochem., 53, 469-500.

Culler, R.L., Graf, J.L., 1984. Rare earth elements in igneous rocks of the continental crust: predominantly basic and ultrabasic rocks. In: Henderson, P. (Ed.), Rare Earth Element Geochemistry. Developments in Geochemistry, 2, Elsevier, Amsterdam, 237-274.

DePaolo, D.J., Linn, A.M., Schubert, G., 1991. The continental crustal age distribution: methods of determining mantle separation ages from Sm-Nd isotopic data and application to the Southwestern United States. J. Geophys. Res., B96, 2071-2088.

Frost, R.B., Barnes, C.G., Collins, W.J., Arculus, R.J., Ellis, D.J., Frost, C.D., 2001. A geochemical classification for granitic rocks. J. Petrology, 42, 2033-2048.

Galindo, C., Casquet, C., Rapela, C., Pankhurst, R.J., Baldo, E., Saavedra, J., 2004. Sr, C and O isotope geochemistry and stratigraphy of Precambrian and Lower Paleozoic carbonate sequences from the Western Sierras Pampeanas of Argentina: tectonic implications. Precambrian Res., 131, 55-71.

Griggs, D.T., Turner, F.J., Heard H.C., 1960. Deformation of rocks at 500 to 800ºC. GSA Memoir, 79, 39-105.

Loewy, S.L., Connelly, J.N., Dalziel, I.W.D., Gower, C.F., 2003. Eastern Laurentia in Rodinia: constraints from whole-rock Pb and U/Pb geochronology. Tectonophysics, 375, 169-197.

Loewy, S.L., Connelly, J.N., Dalziel, I.W.D., 2004. An orphaned basement block: the Arequipa–Antofalla Basement of the central Andean margin of South America. GSA Bulletin, 116, 171-187.

Ludwig, K.R., 1999. Isoplot /Ex Version 2.31, a geochronological toolkit for Microsoft Excel. Berkeley Geochronological Center Special Publication, 1, 2455 Ridge Road, Berkeley, Ca 94709. USA.

Ludwig, K.R., 2001. SQUID 1.02. A user´s manual. Berkeley Geochronological Center Special Publication, 2, 2455 Ridge Road, Berkeley, Ca 94709, USA.

Lucassen, F., Becchio, R., 2003. Timing of high-grade metamorphism: Early Palaeozoic U–Pb formation ages of titanite indicate long-standing high-T conditions at the western margin of Gondwana (Argentina, 26-29ºS). J. Metamorphic Geol., 21, 649-662.

McLennan, S.M., Taylor, S.R., 1979. Rare earth element mobility associated with uranium mineralisation. Nature, 282, 247-250.

Middlemost, E., 1997. Magmas, rocks and planetary development. A survey of magma/igneous rock systems. Longman, London and New York, 299 pp.

Miller, C.F., Mc Dowell, S.M., Mapes, R.W., 2003. Hot and cold granites? Implications of zircon saturation temperatures and preservation of inheritance. Geology, 31, 529–532.

Mulcahy, S.R., Roeske, S.M., McCleland, W.C., Nomade, S., Renne, P.R., 2007. Cambrian initiation of the Las Pirquitas thrust on the western Sierras Pampeanas, Argentina: Implications for the tectonic evolution of the proto-Andean margin of South America. Geology, 35, 443-446.

Nakamura, N., 1974. Determination of REE, Ba, Fe, Mg, Na and K in carbonaceous and ordinary chondrites. Geochim. Cosmochim. Acta, 38, 757-775.

Nelson, D.R., Chivas, A.R., Chappell, B.W., McCulloch, M.T., 1988. Geochemical and isotopic systematics in carbonatite and implications for the evolution of ocean-island sources. Geochim. Cosmochim. Acta, 52, 1–7.

Porcher, C.C., Fernandes, L.A.D., Vujovich, G.I., Chernicoff, C.J., 2004. Thermobarometry, Sm/Nd ages and geophysical evidence for the location of the suture zone between Cuyania and Pampia terranes. In: Vujovich, G.I., Fernandes, L.A.D., Ramos, V.A. (Eds.), Cuyania: an exotic block to Gondwana. Gondwana Res., 7, 1057-1076.

Ramos, V.A., 2004. Cuyania, an exotic block to Gondwana: Review of a historical success and the present problems. In: Vujovich, G.I., Fernandes, L.A.D., Ramos, V.A. (Eds.), Cuyania: An exotic block to Gondwana. Gondwana Res., 7, 1009-1026.

Rapela, C.W., Pankhurst, R.J., Casquet, C., Baldo, E., Saavedra, J., Galindo, C., Fanning, C.M., 1998. The Pampean orogeny of the southern proto-Andes: Cambrian continental collision in the Sierras de Córdoba. In: Pankhurst, R.J., Rapela, C.W. (Eds), The Proto-Andean Margin of Gondwana. Geol. Soc. London, Special Publications, 142, 181-217.

Rapela, C.W., Pankhurst, R.J., Casquet, C., Baldo, E., Saavedra, J., Galindo, C., 1998. Early evolution of the proto-Andean margin of South America. Geology, 26, 707-710.

Rapela C. W., Casquet, C., Baldo, E., Dahlquist, J., Pankhurst, R.J., Galindo, C., Saavedra, J., 2002. Orogénesis del Paleozoico Inferior en el margen proto-andino de Gondwana . Sierras Pampeanas Argentina). J. Iberian Geol., 27, 23-41.

Rapela, C.W., Pankhurst, R.J., Casquet, C., Fanning, C.M., Galindo, C., Baldo, E., 2005. Datación U–Pb SHRIMP de circones detríticos en para-anfibolitas neoproterozoicas de la secuencia Difunta Correa (Sierras Pampeanas Occidentales, Argentina). Geogaceta, 38, 227-230.

Rapela, C.W., Pankhurst, R.J., Casquet, C., Fanning, C.M., Baldo, E., Gonzalez-Casado, J.M., Galindo, C., Dahlquist, J.A., 2007. The Río de La Plata craton and the assembly of SW Gondwana. Earth-Sci. Rev., 83, 49-82.

Schwartz, J.J., Gromet, L.P., 2004. Provenance of Late Proterozoic - Early Cambrian basin, Sierras de Córdoba, Argentina. Precambrian Res., 129, 1-21.

Schultz, F., Lehmann, B., Tawackoli, S., Rossling, R., Belyatsky, B., Dulski, P., 2004. Carbonatite diversity in the Central Andes: The Ayopaya alkaline province, Bolivia. Contrib. Mineral. Petrol., 148, 391–408.

Thomas, W.A., 1991. The Appalachian – Ouachita rifted margin of southeastern North America. GSA Bulletin, 103, 415-431.

Thomas, W.A., Astini, R.A., 1996. The Argentine Precordillera: a traveler from the Ouachita embayment of North America Laurentia. Science, 273, 752-757.

Thomas, W.A., Astini, R.A., 2003. Ordovician accretion of the Argentine Precordillera terrane to Gondwana: a review. J. South Am. Earth Sci., 16, 67-79.

Thompson, R.N., 1982. British Tertiary volcanic province. Scottish J. Geol., 18, 49-107.

Tohver, E., van der Pluijm, B.A., Van der Voo, R., Rizzotto, G., Scandolara, J.E., 2002. Paleogeography of the Amazon craton at 1.2 Ga: early Grenville collision with the llano segment of Laurentia. Earth Planet. Sci. Lett., 199, 185-200.

Tohver, E., Bettencourt, J.S., Tosdal, R., Mezger, K., Leite, W.B., Payolla, B.L., 2004. Terrane transfer during the Grenville orogeny: tracing the Amazonian ancestry of southern Appalachian basement through Pb and Nd isotopes. Earth Planet. Sci. Lett., 228, 161-176.

Trindade, R.I.F., D´Agrella-Filho, M.S., Epof, I., Brito Neves, B.B., 2006. Paleomagnetism of Early Cambrian Itabaiana mafic dikes (NE Brazil) and the final assembly of Gondwana. Earth Planet. Sci. Lett., 244, 361-377.

Varela, R., Sato, A., Bassei, M.A.S., Siga Jr, O., 2003. Proterozoico medio y Paleozoico inferior de la Sierra de Umango, antepais andino (29º S), Argentina: edades U–Pb y caracteristicas isotópicas. Revista Geol. Chile, 30, 265-284.

Vaughan, A.P.M., Pankhurst, R.J., 2008. Tectonic overview of the West Gondwana margin. Gondwana Res., 13, 150–162.

Vaughan, A.P.M., Scarrow, J.H., 2003. K-rich mantle metasomatism control of localization and initiation of lithospheric strike-slip faulting. Terra Nova, 15, 163–169.

Veevers, J.J., 2003. Pan-African is Pan-Gondwanaland: Oblique convergence drives rotation during 650-500Ma assembly. Geology, 31, 501-504.

Veevers, J.J., 2007. Pan-Gondwanaland post-collisional extension marked by 650-500 Ma alkaline rocks and carbonatites and related detrital zircons: A review. Earth-Sci. Rev., 83, 1-47.

Villenueve, M.E., Relf, C., 1998. Tectonic setting of 2.6 Ga carbonatites in the Slave Province, NW Canada. J. Petrology, 39, 1975-1986.

Vujovich, G.I., Kay, S.M., 1998. A Laurentian? Grenville-age oceanic arc/back-arc terrane in the Sierra de Pie de Palo, Western Sierras Pampeanas, Argentina. In: Pankhurst, R.J., Rapela, C.W. (Eds.) The Proto-Andean margin of Gondwana. Geol. Soc. London, Special Publication, 142, 159-180.

Vujovich, G.I., Van Staal, C.R., Davis, W., 2004. Age constraints and the tectonic evolution and provenance of the Pie de Palo Complex, Cuyania composite terrane, and the Famatinian orogeny in the Sierra de Pie de Palo, San Juán, Argentina. Gondwana Res., 7, 1041-1056.

Watson, E.B., 1979. Zircon saturation in felsic liquids: experimental results and applications to trace element geochemistry. Contrib. Mineral. Petrol., 70, 407–419.

Watson, E.B., Harrison, T.M., 1983. Zircon saturation revisited: Temperature and composition effects in a variety of crustal magma types. Earth Planet. Sci. Lett., 64, 295–304.

Williams, I.S., 1998. U-Th-Pb geochronology by ion microprobe. In: McKibben, M.A., Shanks, W.C. III, Ridley, W.I. (Eds.), Applications of microanalytical techniques to understanding mineralizing processes. Rev. Econ. Geol., 7, 1-35.

Wingate, M.T.D., Campbell, I.H., Compston, W., Gibson, G.M., 1998. Ion microprobe U–Pb ages for Neoproterozoic-basaltic magmatism in south-central Australia and implications for the breakup of Rodinia. Precambrian Res., 87, 135-159.

Figure captions

Figure 1. (a) Sketch map of the Sierras Pampeanas (light grey) and the Argentine Precordillera (PRE) (dark grey). (A) Ancasti, (Ch) Chepes, (Co) Córdoba, (F) Famatina, (PP) Pié de Palo, (SL) San Luís, (UME), Umango, Maz and Espinal, (V) Velasco. Mobile belts where either Grenville-age (1.0 – 1.2 Ga), Pampean (540 – 520 Ma) or Famatinian (490 – 435 Ma) deformation and metamorphism predominate are distinguished. (b) Geological sketch map of the Sierra del Maz and surrounding areas based on Casquet et al., (2006). The box indicates the location of the study area.

Figure 2. Geological map of NE Sierra de Maz based on fieldwork and interpretation of satellite raster images.

Figure 3. (a) South-facing view of the carbonatite – syenite body at its contact with the host Grenville-age gneisses and amphibolites. A screen of gneisses is visible in the centre of the image, view width ca. 100 m. (b) Rounded coarse-grained syenite enclave wrapped in a weak foliated carbonatite matrix. (c) Very poorly-sorted and weakly-foliated breccia. Clasts consist of syenite and gneiss. The large gneiss clast is discordant to the carbonatite foliation which is

parallel to the knife. (d) Carbonatite breccia. Unorientated, moderately-sorted, rounded syenite clasts in carbonatite matrix. (e) Two-stage breccia. Poorly-sorted syenite breccia (angular clasts), sharply bounded by a well-sorted weakly foliated microbreccia. Matrix is carbonatite in both facies. (f) Coarse-grained syenite with large euhedral zircon crystals.

Figure 4. (a) Nomenclature of plutonic rocks and different suite lineages, after Middlemost (1997). (b) FeOt/(FeOt + MgO) *vs.* SiO_2 wt. %, showing the Frost et al., (2001) boundary between ferroan and magnesian plutonic rocks, as well as the field of A-type granites. (c) Plot of $Na_2O + K_2O - CaO$ against SiO_2 wt. % for the syenitic suite of Sierra de Maz. Limits for the rock series and field of A-type granites are from Frost et al., (2001).

Figure 5. Plot of Zr *vs.* $N_{a2}O + K_2O/Al_2O_3$ (mol) for the syenitic suite of Sierra de Maz.

Figure 6. Eu/Eu*, P_2O_5, Sr and Y *vs.* SiO_2 wt. % for the syenitic suite of Sierra de Maz.

Figure 7. (a) Chondrite-normalized REE abundances of the syenitic suite of the Sierra de Maz complex. (b) Selected REE patterns of apatite, zircon and plagioclase from alkaline rocks and U-rich granites, from Bea (1996). Note that a modelled REE pattern for a rock with 1.9% of normative apatite closely resembles the pattern of the least evolved member of the syenitic suite (sample MAZ-12110). (c) REE, Sr and Zr plot of two silico-carbonatite samples from the Sierra de Maz complex. The open circle represents a single homogeneous crystal of carbonate separated from the carbonatite. The general carbonatite field is taken from13 samples reported by Nelson et al., (1988), whereas open squares are carbonatites reported by Villeneuve and Relf (1998). Data are normalized to chondritic values of Nakamura (1974);

other normalizing data from Boynton (1984) for Tb, Ho, Tm, and Sr and Thompson (1982) for Zr.

Figure 8. Rb-Sr isochron plot of whole-rock samples from the Maz carbonatite and syenite complex

Figure 9. (a) back-scattered electron image of zircon in thin-section of syenite sample MAZ-12085, showing complex internal structure of a euhedral grain. NB in the latter image the dark areas are those relatively depleted in U and REE, whereas in the CL images such composition result in high luminescence. (b) cathodo-luminescence (CL) image of part of the analysed zircon megacryst from the Sierra de Maz syenite, showing the complex internal structure and the U–Pb ages determined from SHRIMP analyses. (c) CL image of typical fragmented crystals of zircon separated from syenite sample MAZ-12057, together with the U–Pb ages obtained from SHRIMP analyses.

Figure 10. (a) Tera-Wasserburg plot of U–Pb SHRIMP data for the zircon megacryst extracted from the syenite (Fig. 9b), error ellipses are 95% confidence limits; (b) Probability density plot (Ludwig 1999) of ^{207}Pb-corrected ^{206}Pb–^{238}U ages. Shading reflects groupings identified in the text.

Figure 11. (a) Tera-Wasserburg plot of U–Pb SHRIMP data for separated zircon from MAZ-12057 (Fig. 9c), error ellipses are 95% confidence limits; (b) Probability density plot (Ludwig 1999) of ^{207}Pb-corrected ^{206}Pb–^{238}U ages. Shading reflects groupings identified in the text.

Figure 12. a) The Clymene ocean separated a large continental mass that embraced Amazonía (AM), the Western Sierras Pampeanas (WSP), and the Arequipa-Antofalla craton (AAC) among others, from eastern Gondwana cratons (KC: Kalahari craton; RPC: Rio de la Plata craton). The Maz syenite – carbonatite body was intruded at ca. 570 Ma at the southern tip of this continental mass. Emplacement took place during early continental rifting that eventually led to opening of the Clymene Ocean. The Puncoviscana Formation was deposited on the eastern side of the Clymene Ocean (present coordinates), b) Oblique right-lateral collision produced the Pampean orogeny between 540 and 520 Ma. Paleogeographic model according to Rapela et al. (2007).

Table

Table 1. Representative chemical analyses of the Sierra de Maz carbonatite-syenite suite

Samples	MAZ12110	MAZ12085	MAZ-12058	MAZ-12057	MAZ-13004	MAZ-13017	MAZ-12090
		Syenitic suite			*Carbonatites*		*Calcite megacryst*
Major oxides (wt%)							
SiO_2	52.59	58.46	61.14	64.05	18.18	19.97	0.04
TiO_2	0.28	0.2	0.44	0.35	0.75	2.08	0
Al_2O_3	19.88	22.91	19.71	19.38	5.93	6.71	0.01
Fe_2O_3	0.46	0.39	1.99	0.21	10.38	13.29	2.74
FeO[1]	2.55	1.84	2.89	3.38	nd	nd	nd
MnO	0.08	0.04	0.07	0.05	0.96	0.33	1.28
MgO	0.56	0.29	0.44	0.23	2	3.4	0.42
CaO	5.55	1.7	1.02	0.58	32.38	28.06	69.11
Na_2O	7.92	9.37	7.87	9.02	1.63	1.33	0.08
K_2O	3.77	2.52	2.79	2.09	1.23	2.49	0.01
P_2O_5	0.74	0.15	0.14	0.02	2.15	2.57	0.02
LOI	4.94	1.41	0.78	0.67	24.24	19.61	nd
CO_2	nd	nd	nd	nd	24.5	19.7	nd
F	nd	nd	nd	nd	0.19	0.17	nd
Cl	nd	nd	nd	nd	0.04	0.03	nd
SO_3	nd	nd	nd	nd	0	0	0.02
Total S	nd	nd	nd	nd	0.07	0.03	nd
TOTAL	99.32	99.28	99.28	100.03	100.14	100.03	73.73
Trace elements (ppm)							
Cs	1.1	2.6	1.1	0.8	1.2	1.7	61
Rb	132	78	116	69	70	140	28
Sr	1702	1476	1135	1120	6248	6480	11086
Ba	886	1161	896	1041	635	2028	759
La	41.8	11	3.99	0.8	287	463	1067
Ce	94.2	23.4	9.86	1.3	581	901	2043
Pr	11	2.63	1.27	0.13	64.3	96.8	nd
Nd	40.8	9.81	5.01	0.44	249	380	856
Sm	7.24	1.71	0.94	0.08	46.2	64.9	141
Eu	2.47	0.74	0.58	0.14	15	20	nd
Gd	6.07	1.57	0.89	0.08	36.5	47.2	nd
Tb	0.87	0.25	0.13	0.02	5.83	7.04	nd
Dy	4.23	1.46	0.71	0.12	29.4	33.1	nd
Ho	0.69	0.29	0.15	0.03	4.83	5.22	nd
Er	1.68	0.79	0.47	0.14	12.8	12.8	nd
Tm	0.2	0.11	0.07	0.03	1.66	1.49	nd
Yb	1.07	0.67	0.54	0.23	9.47	7.8	27
Lu	0.14	0.09	0.1	0.04	1.34	1.01	nd
U	8.31	12.2	0.77	0.93	2.65	1.85	42
Th	1.44	4.31	0.33	0.25	0.93	4.26	21
Y	17.3	7	3.6	1	150	157	393
Nb	90.8	53.5	119	107	360	93.3	nd
Zr	764	1920	1338	716	226	298	39
Hf	19.3	27.4	25.2	11	3	4.1	37
Ta	31	11	9.3	12.7	16.7	5.2	nd
Ga	16	21	18	21	21	24	nd
Ge	1	0.7	1	0.9	1.4	1.9	nd

Major oxides were determined by ICP and trace elements were determined by ICP-MS at ACTLABS, Canada.
Fe determined volumetrically at CIG, La Plata. LOI = loss on ignition

Table

Table 2. Sr and Nd Isotopic Data for Sierra de Maz Syenite–Carbonatite Complex.

Sample		**Rb ppm**	**Sr ppm**	**Rb/Sr**	**^{87}Rb/^{86}Sr**	**^{87}Sr/^{86}Sr**	**^{87}Sr/^{86}Sr$_0$**	**Sm ppm**	**Nd ppm**	**Sm/Nd**	**^{147}Sm/^{144}Nd**	**^{143}Nd/^{144}Nd**	**^{143}Nd/^{144}Nd$_0$**	**εNd$_0$**	**T$_{DM}$**	**T$_{DM}$***
MAZ 12057	Syenite	69	1120	0.0616	0.1782	0.704456	0.70301	0.08	0.44	0.1818						
MAZ 12058	Ne-syenite	116	1135	0.1022	0.2956	0.704837	0.70243	0.94	5.01	0.1876						
MAZ 12085	Ne-syenite	78	1476	0.0528	0.1528	0.704216	0.70297	1.71	9.81	0.1743	0.1054	0.512474	0.512080	3.5	837	970
MAZ 12110	Ne-syenite	132	1702	0.0776	0.2243	0.704482	0.70266	7.24	40.8	0.1775	0.1073	0.512486	0.512085	3.6	835	961
MAZ-12056	carbonatite calcite	11.884	3108	0.0038	0.0111	0.702997	0.70291	23.13	95.10	0.2432	0.1470	0.512741	0.512192	5.6	760	764
MAZ-12086	carbonatite calcite	6.951	4211	0.0017	0.0048	0.703056	0.70302	24.63	91.84	0.2682	0.1621	0.512756	0.512150	4.8	913	843
MAZ-11001	carbonatite calcite	13.015	8493	0.0015	0.0044	0.703000	0.70296	22.37	91.72	0.2439	0.1474	0.512622	0.512072	3.3	1005	986
MAZ-12061	Biotite megracryst	393	106	3.7240	10.8494	0.778719	*0.69055*									
MAZ-12107	Biotite megracryst	854	503	1.6983	4.9275	0.736679	*0.69663*									
MAZ-12059	Aegirine mafic enclave	3.421	781	0.0044	0.0127	0.703175	0.70307									
MAZ-12060	Albite megacryst	6.797	1557	0.0044	0.0126	0.703168	0.70307									
MAZ-12090b	Vein calcite					0.702772										
MAZ-12090a	Vein calcite					0.702757										

Sr and Nd isotopic ratios were normalized to ^{86}Sr/^{88}Sr = 0.1194 and ^{146}Nd/^{144}Nd = 0.7219, respectively.
NBS987 standard gave a mean ^{87}Sr/^{86}Sr ratio of 0.710234 ± 0.00005 (n = 12) and La Jolla Nd standard gave a mean ^{143}Nd/^{144}Nd of 0.511861 ± 0.00002 (n = 2).
The 2σ analytical errors are 1% in ^{87}Rb/^{86}Sr, 0.1% in ^{147}Sm/^{144}Nd, 0.01% in ^{87}Sr/^{86}Sr and 0.006% in ^{143}Nd/^{144}Nd
Decay constants used were λRb = 1.42x10-11 a-1 and λSm = 6.54x10-12 a-1.
T$_{DM}$* is model age according to DePaolo *et al.* (1991).
^{147}Sm/^{144}Nd and ^{143}Nd/^{144}Nd values assumed to be 0.1967 and 0.512636 for CHUR, and 0.222 and 0.513114 for depleted mantle respectively

Table

Table 3. U-Pb SHRIMP data for zircon

Spot	U (ppm)	Th (ppm)	Th/U	$^{206}Pb^*$ (ppm)	$^{204}Pb/^{206}Pb$	f_{206} %	Total $^{238}U/^{206}Pb$	±	Total $^{207}Pb/^{206}Pb$	±	Radiogenic $^{206}Pb/^{238}U$	±	Age (Ma) $^{206}Pb/^{238}U$	±
(a) Megacryst in syenite (MAZ-12089).														
1	331	313	0.95	22.7	0.00011	0.21	12.5123	0.1391	0.0588	0.0005	0.0798	0.0009	494.6	5.4
2	36	10	0.28	2.4	0.00018	0.02	12.9951	0.2427	0.0568	0.0019	0.0769	0.0015	477.8	8.8
3	39	17	0.44	2.4	0.00099	0.64	13.8073	0.2510	0.0611	0.0023	0.0720	0.0013	448.0	8.1
4	448	203	0.45	26.8	0.00006	0.16	14.3597	0.1565	0.0568	0.0005	0.0695	0.0008	433.3	4.6
5	88	14	0.16	6.9	-	0.41	10.9412	0.1545	0.0622	0.0012	0.0910	0.0013	561.6	7.8
6	22	5	0.23	1.7	0.00097	0.88	10.9459	0.2411	0.0659	0.0024	0.0906	0.0020	558.8	12.1
7	595	486	0.82	38.3	-	0.19	13.3401	0.1427	0.0579	0.0004	0.0748	0.0008	465.1	4.9
8	1115	1086	0.97	88.9	0.00002	0.05	10.7726	0.1118	0.0596	0.0003	0.0928	0.0010	571.9	5.8
9	405	92	0.23	29.7	0.00005	<0.01	11.6974	0.1293	0.0576	0.0005	0.0855	0.0010	529.0	5.7
10	36	9	0.25	2.8	0.00090	0.54	11.0190	0.2023	0.0632	0.0018	0.0903	0.0017	557.1	10.1
11	453	66	0.15	33.8	0.00001	0.16	11.5392	0.1260	0.0595	0.0006	0.0865	0.0010	534.9	5.7
12	94	36	0.38	7.4	0.00023	<0.01	10.9050	0.1517	0.0572	0.0011	0.0919	0.0013	566.8	7.7
13	222	163	0.74	13.3	0.00042	0.33	14.3887	0.1729	0.0582	0.0008	0.0693	0.0008	431.7	5.1
14	27	4	0.15	2.1	0.00135	<0.01	10.9319	0.2272	0.0563	0.0023	0.0918	0.0020	566.0	11.6
15	56	10	0.17	4.6	0.00033	<0.01	10.4643	0.1678	0.0590	0.0024	0.0956	0.0016	588.8	9.4
16	163	39	0.24	12.6	0.00003	0.17	11.0752	0.1378	0.0601	0.0009	0.0901	0.0011	556.4	6.8
17	369	64	0.17	31.6	0.00009	0.12	10.0324	0.1116	0.0612	0.0006	0.0996	0.0011	611.8	6.6
18	31	7	0.23	2.2	0.00143	0.59	11.9436	0.2403	0.0624	0.0021	0.0832	0.0017	515.4	10.2
19	384	348	0.90	24.7	0.00017	0.26	13.3870	0.1725	0.0584	0.0006	0.0745	0.0010	463.2	5.8
20	500	527	1.05	33.1	0.00007	0.10	12.9963	0.1410	0.0574	0.0005	0.0769	0.0008	477.4	5.1
Error in Temora reference zircon calibration was 0.65% for the analytical session (not included in above errors but required when comparing data from different mounts).														
(a) Zircon grains from syenite sample MAZ-12057.														
1.1	132	31	0.23	9.6	0.00019	0.17	11.8406	0.1381	0.0592	0.0008	0.0843	0.0010	521.8	6.0
2.1	156	63	0.41	12.3	0.00011	<0.01	10.9227	0.1246	0.0589	0.0007	0.0916	0.0011	564.7	6.3
3.1	51	11	0.22	4.2	-	0.19	10.5115	0.2263	0.0611	0.0018	0.0949	0.0021	584.7	12.3
4.1	15	2	0.11	1.1	0.00084	0.25	11.7823	0.2423	0.0599	0.0026	0.0847	0.0018	523.9	10.6
5.1	65	17	0.26	5.3	0.00009	0.04	10.5699	0.1380	0.0598	0.0011	0.0946	0.0013	582.5	7.4
6.1	508	513	1.01	41.4	0.00003	0.04	10.5318	0.1107	0.0598	0.0004	0.0949	0.0010	584.5	6.0
7.1	159	48	0.30	12.8	-	0.13	10.6742	0.1551	0.0603	0.0007	0.0936	0.0014	576.6	8.2
8.1	82	25	0.31	6.5	0.00030	0.11	10.9082	0.1648	0.0599	0.0012	0.0916	0.0014	564.8	8.4
9.1	226	117	0.52	18.5	0.00003	<0.01	10.4898	0.1158	0.0594	0.0005	0.0954	0.0011	587.1	6.3
10.1	28	5	0.17	2.1	-	<0.01	11.8505	0.4234	0.0537	0.0015	0.0848	0.0031	524.8	18.3
11.1	104	31	0.30	8.0	0.00024	<0.01	11.1549	0.1404	0.0584	0.0008	0.0897	0.0012	553.6	6.8
12.1	279	141	0.50	22.7	0.00000	0.04	10.5359	0.1144	0.0598	0.0005	0.0949	0.0011	584.3	6.2
13.1	26	5	0.19	1.8	0.00043	<0.01	12.5276	0.2281	0.0570	0.0024	0.0798	0.0015	495.1	8.9
14.1	105	15	0.14	8.1	0.00020	0.09	11.1599	0.1388	0.0593	0.0011	0.0895	0.0011	552.7	6.7
15.1	51	4	0.07	3.9	0.00012	<0.01	11.1513	0.3850	0.0586	0.0018	0.0897	0.0032	553.6	18.7
16.1	463	419	0.91	36.7	-	0.08	10.8333	0.1235	0.0597	0.0004	0.0922	0.0011	568.7	6.3
17.1	70	20	0.29	5.8	0.00015	<0.01	10.4887	0.1365	0.0584	0.0010	0.0955	0.0013	587.8	7.5
18.1	270	129	0.48	21.5	0.00007	<0.01	10.7867	0.1196	0.0582	0.0005	0.0928	0.0011	572.2	6.2
19.1	453	420	0.93	35.9	0.00001	0.01	10.8307	0.1144	0.0591	0.0004	0.0923	0.0010	569.2	5.9
20.1	142	66	0.47	11.0	-	0.20	11.0545	0.1292	0.0604	0.0007	0.0903	0.0011	557.2	6.4
21.1	156	70	0.45	11.4	0.00004	<0.01	11.7096	0.1355	0.0577	0.0007	0.0854	0.0010	528.4	6.0
22.1	34	5	0.15	2.5	0.00062	<0.01	11.3710	0.3692	0.0566	0.0016	0.0881	0.0029	544.5	17.3
24.1	232	104	0.45	18.6	0.00005	<0.01	10.7277	0.1192	0.0585	0.0006	0.0933	0.0011	575.0	6.2
23.1	121	47	0.39	9.3	0.00003	<0.01	11.1435	0.1583	0.0583	0.0008	0.0898	0.0013	554.2	7.7
25.1	50	8	0.17	3.9	-	<0.01	10.9988	0.1673	0.0583	0.0013	0.0910	0.0014	561.3	8.4
26.2	84	19	0.23	6.7	0.00008	<0.01	10.6714	0.1370	0.0587	0.0010	0.0938	0.0012	577.8	7.3
11.3	98	29	0.29	7.1	0.00015	<0.01	11.8105	0.1492	0.0569	0.0009	0.0848	0.0011	524.5	6.5
27.1	71	17	0.24	5.5	-	<0.01	11.0560	0.1478	0.0573	0.0011	0.0906	0.0012	559.2	7.3

Error in Temora reference zircon calibration was 0.59% and 0.61% for the analytical sessions (spots 1-21 and 22-27 respectively
(not included in above errors but required when comparing data from different mounts).
Note that analyses 11.2 and 26.1 were not completed

Notes 1. Uncertainties given at the one σ level.
2. f_{206} % denotes the percentage of ^{206}Pb that is common Pb.
3. Correction for common Pb made using the measured $^{238}U/^{206}Pb$ and $^{207}Pb/^{206}Pb$ ratios

following Tera and Wasserburg (1972) as outlined in Williams (1998).

Figure
Click here to download high resolution image

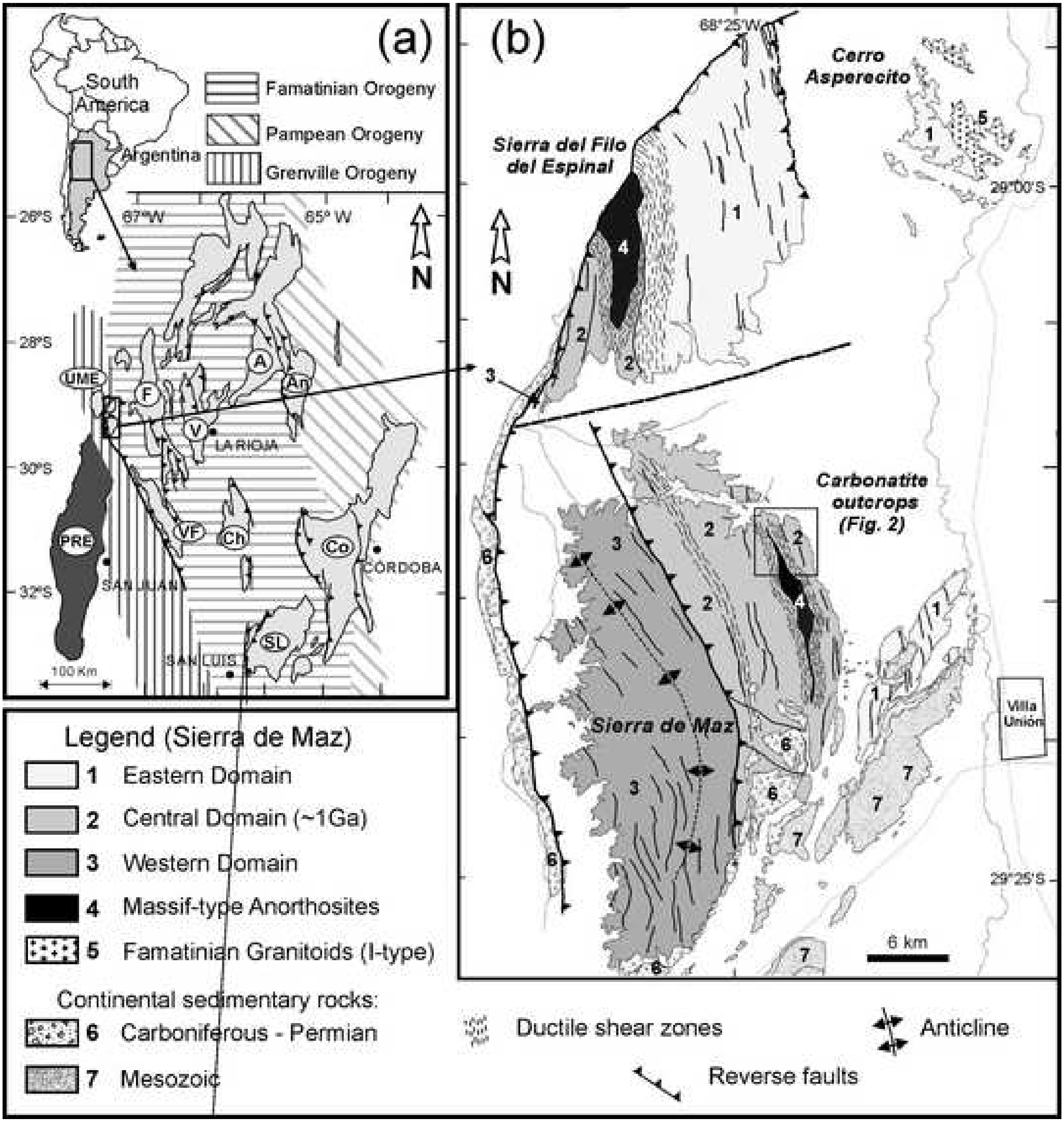

Figure
Click here to download high resolution image

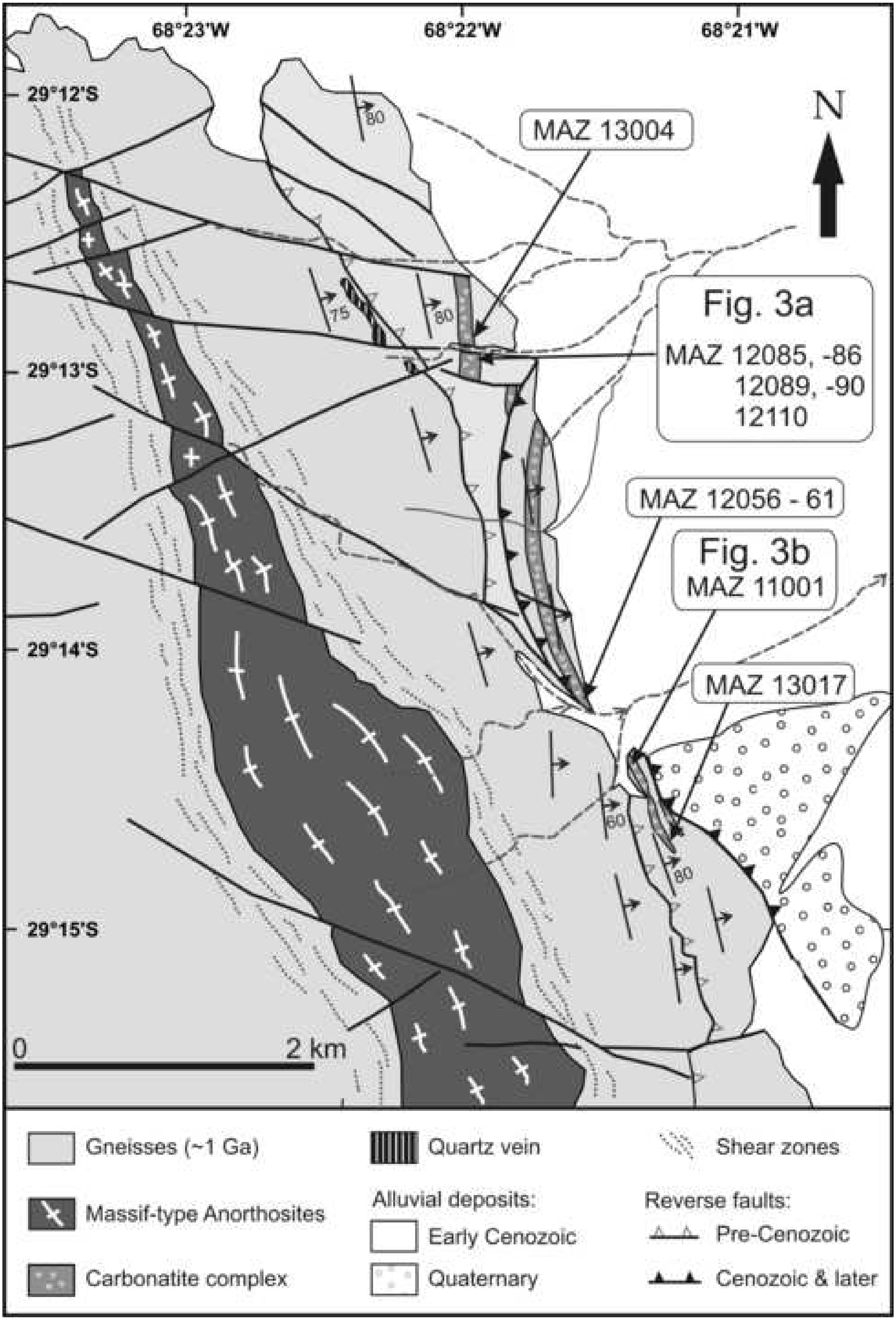

Figure
Click here to download high resolution image

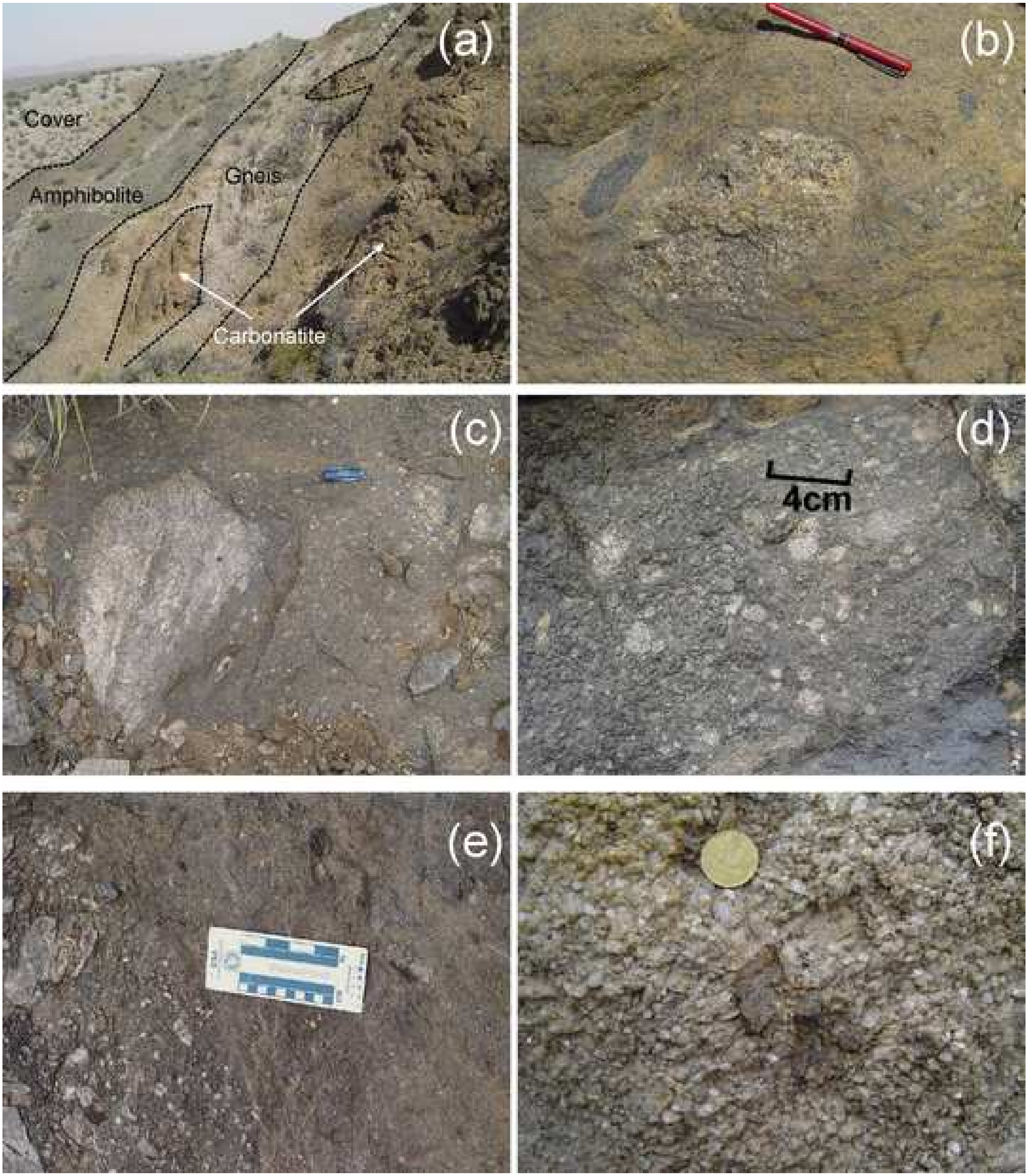

Figure

Click here to download high resolution image

Fig. 4

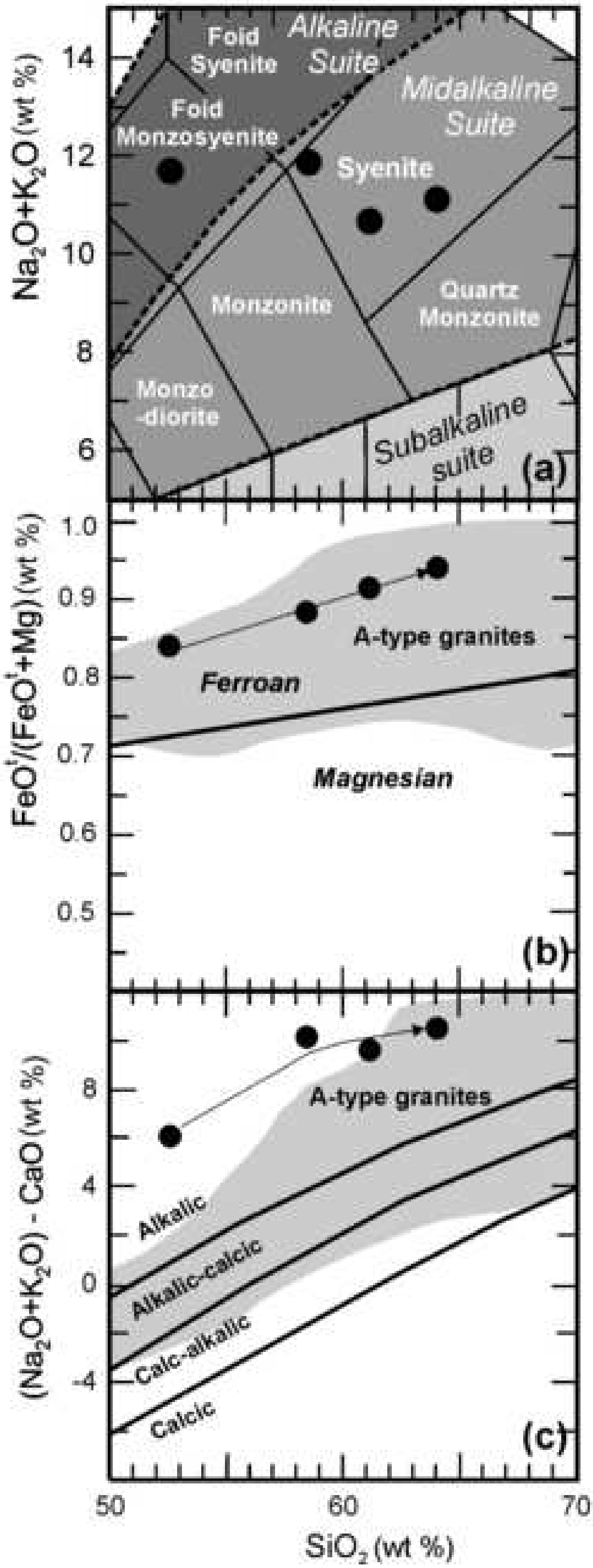

Figure
Click here to download high resolution image

Fig. 5

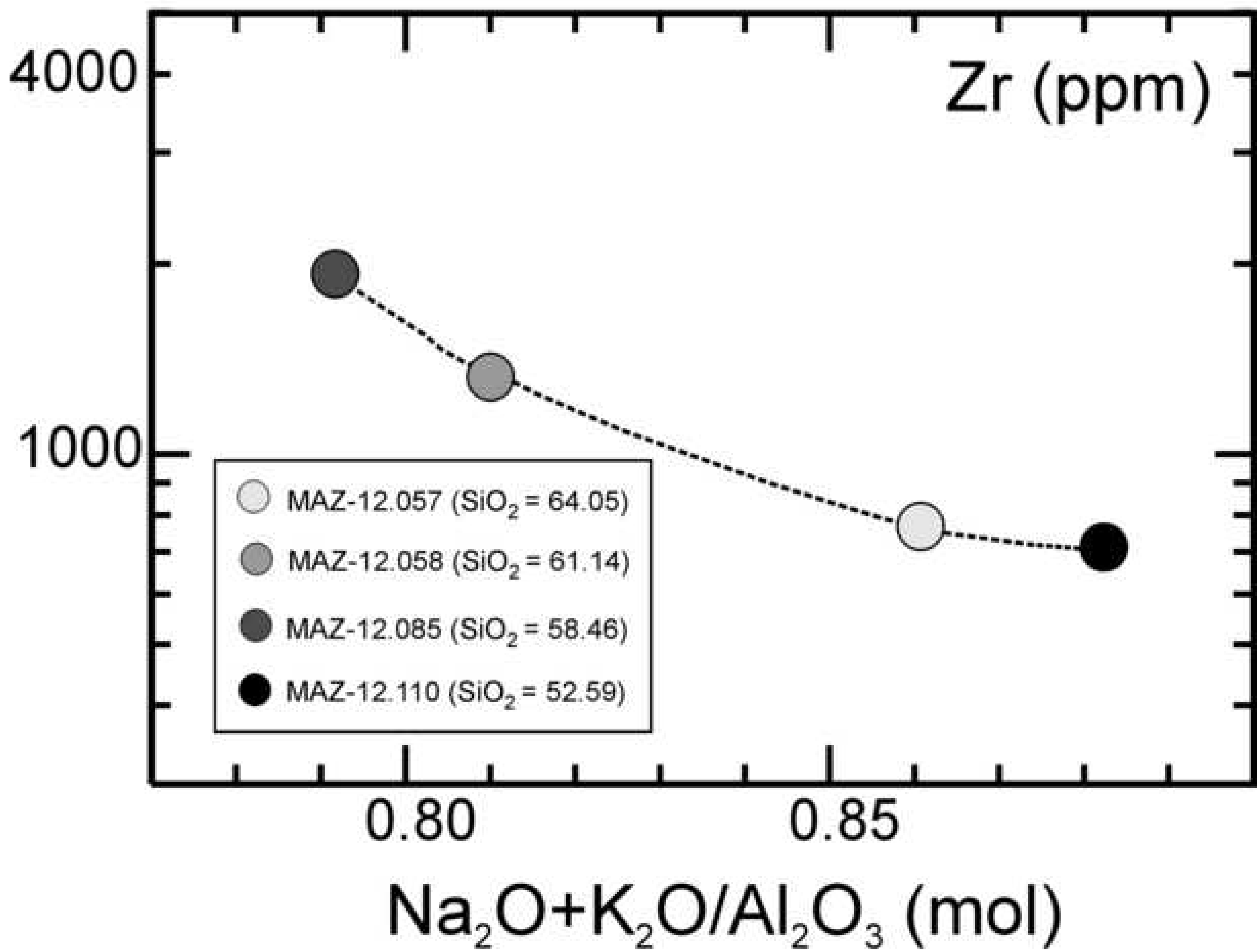

Figure
Click here to download high resolution image

Fig. 6

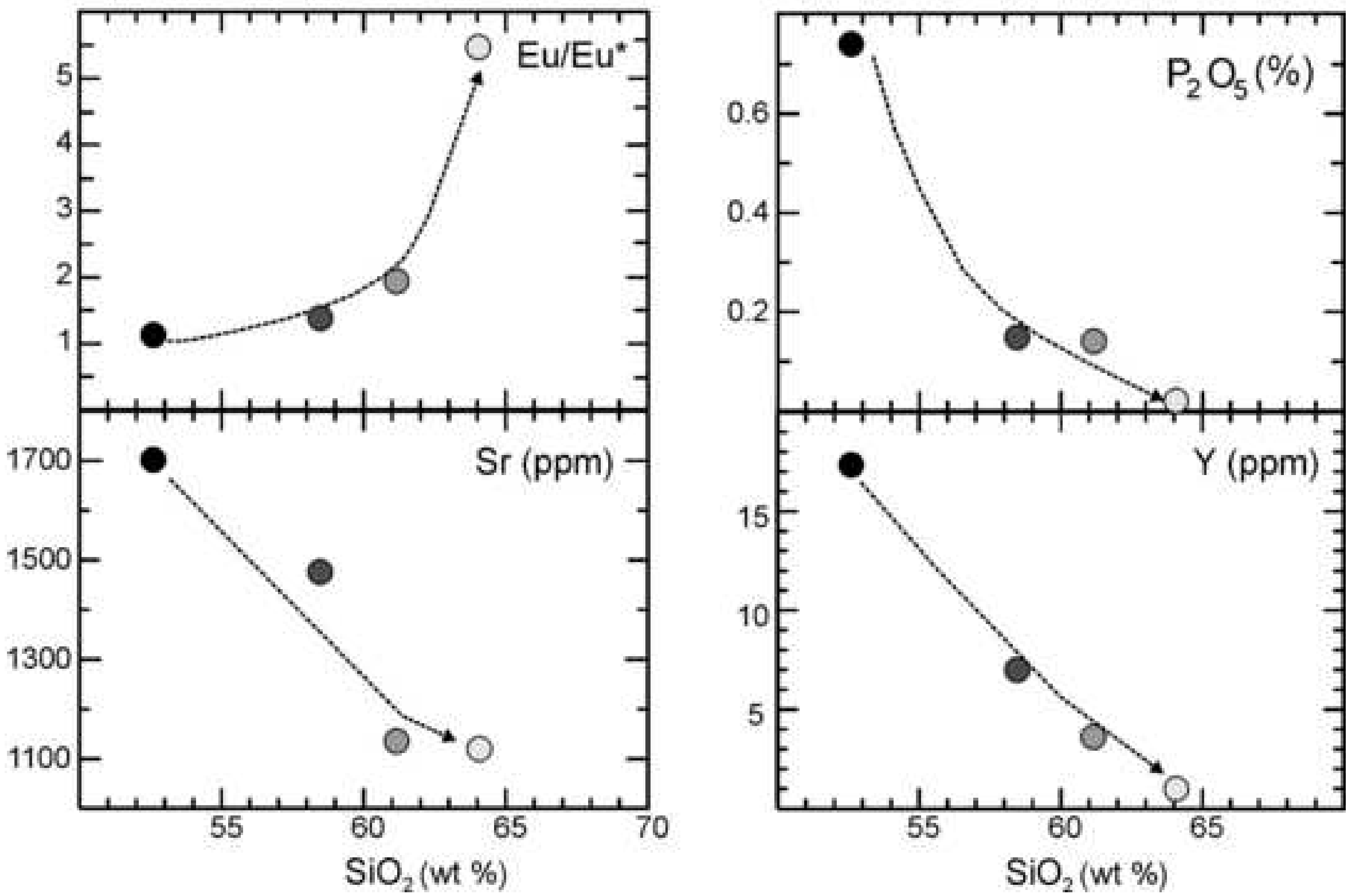

Figure
Click here to download high resolution image

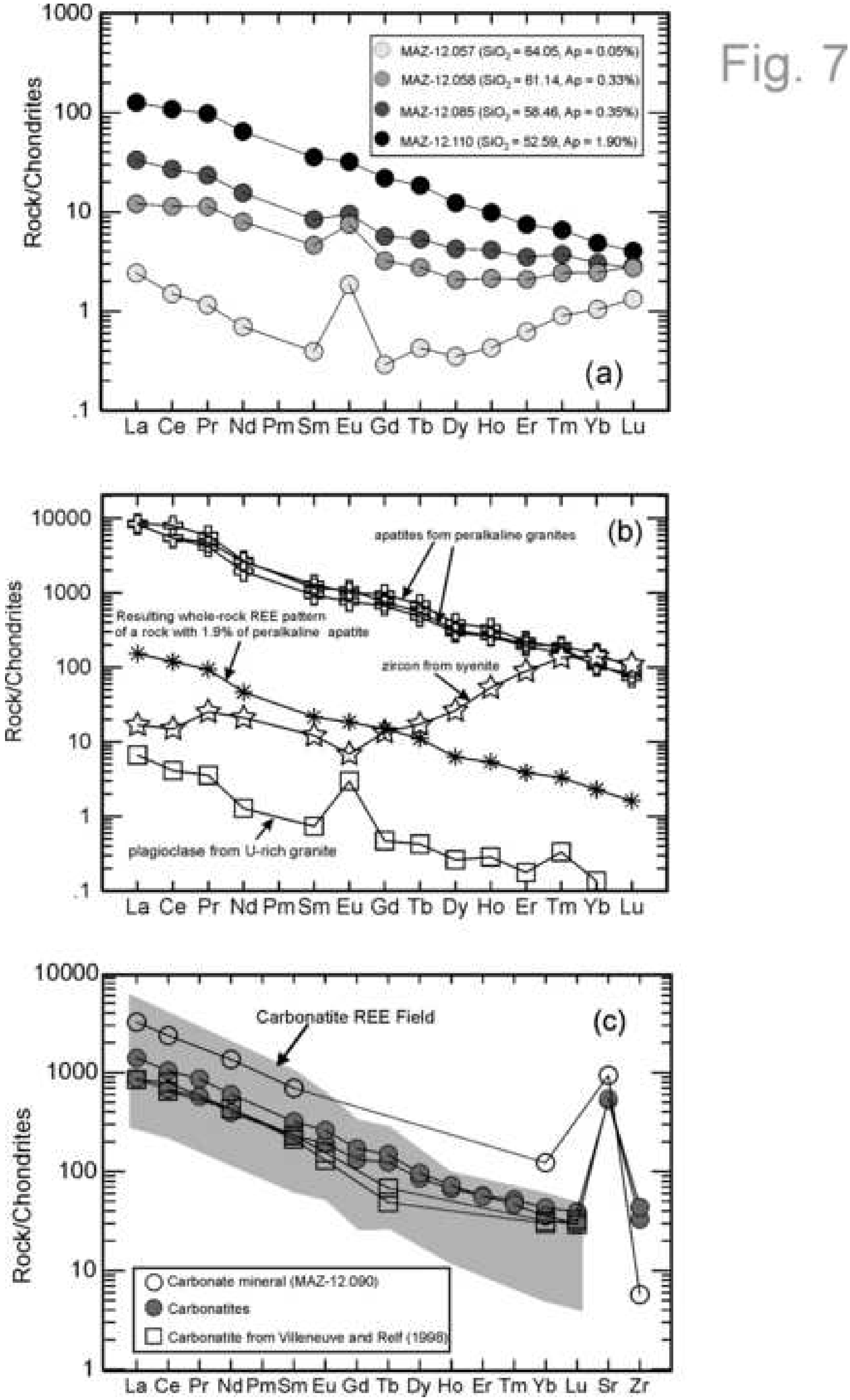

Fig. 8

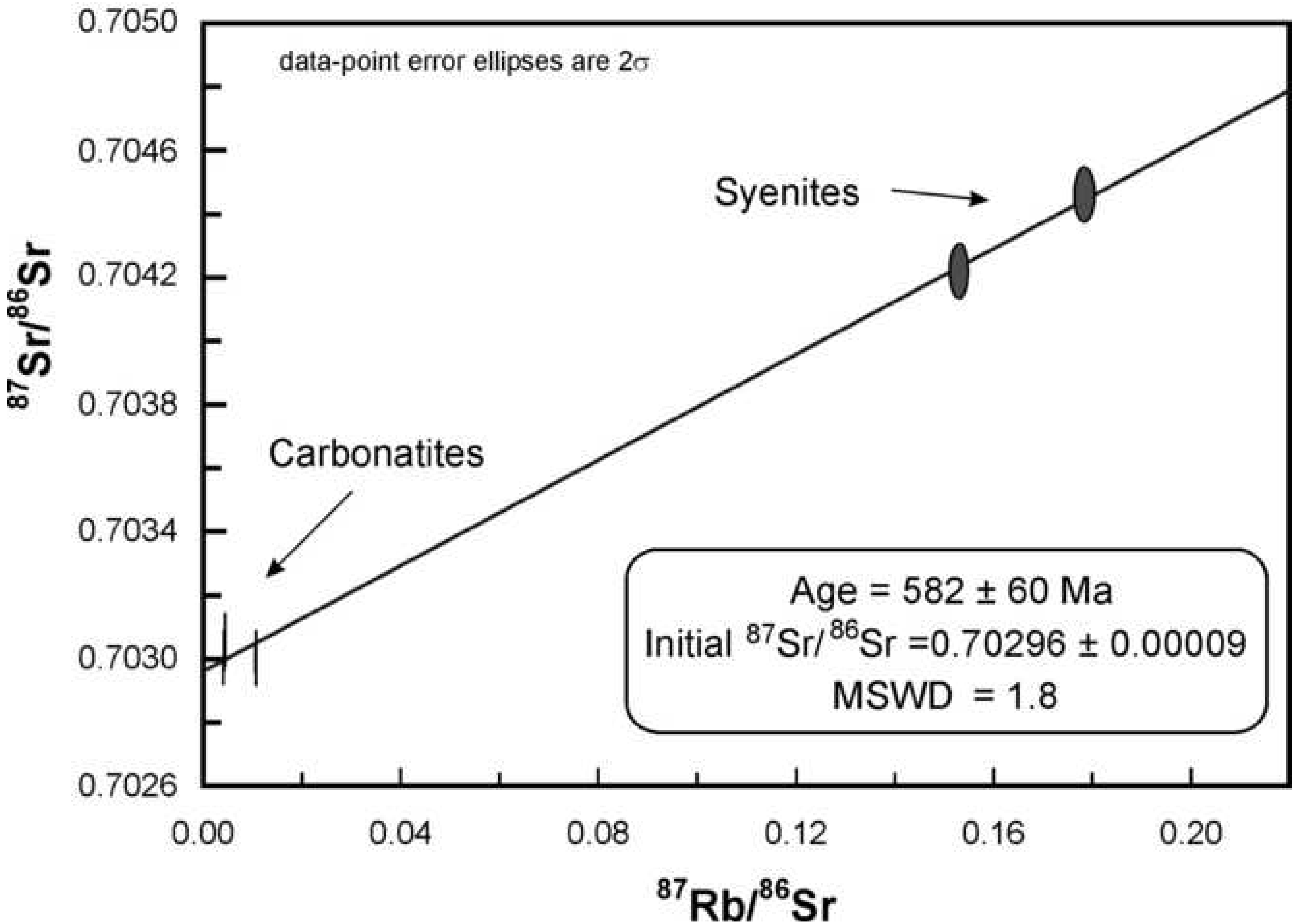
data-point error ellipses are 2σ
Syenites
Carbonatites
Age = 582 ± 60 Ma
Initial $^{87}Sr/^{86}Sr$ =0.70296 ± 0.00009
MSWD = 1.8
$^{87}Sr/^{86}Sr$
0.7050
0.7046
0.7042
0.7038
0.7034
0.7030
0.7026
0.00
0.04
0.08
0.12
0.16
0.20
$^{87}Rb/^{86}Sr$

Figure
Click here to download high resolution image

Fig. 9

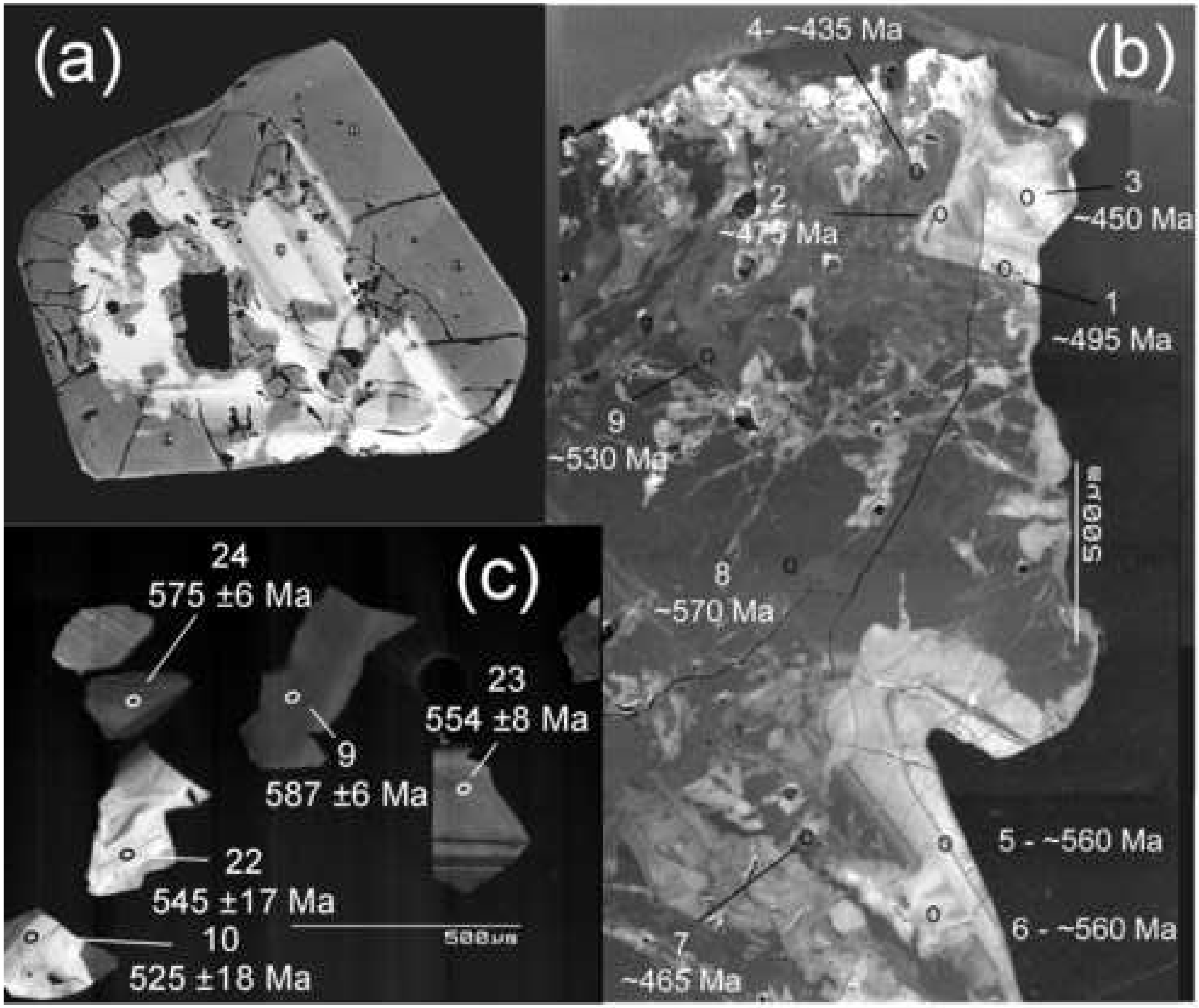

Figure

Click here to download high resolution image

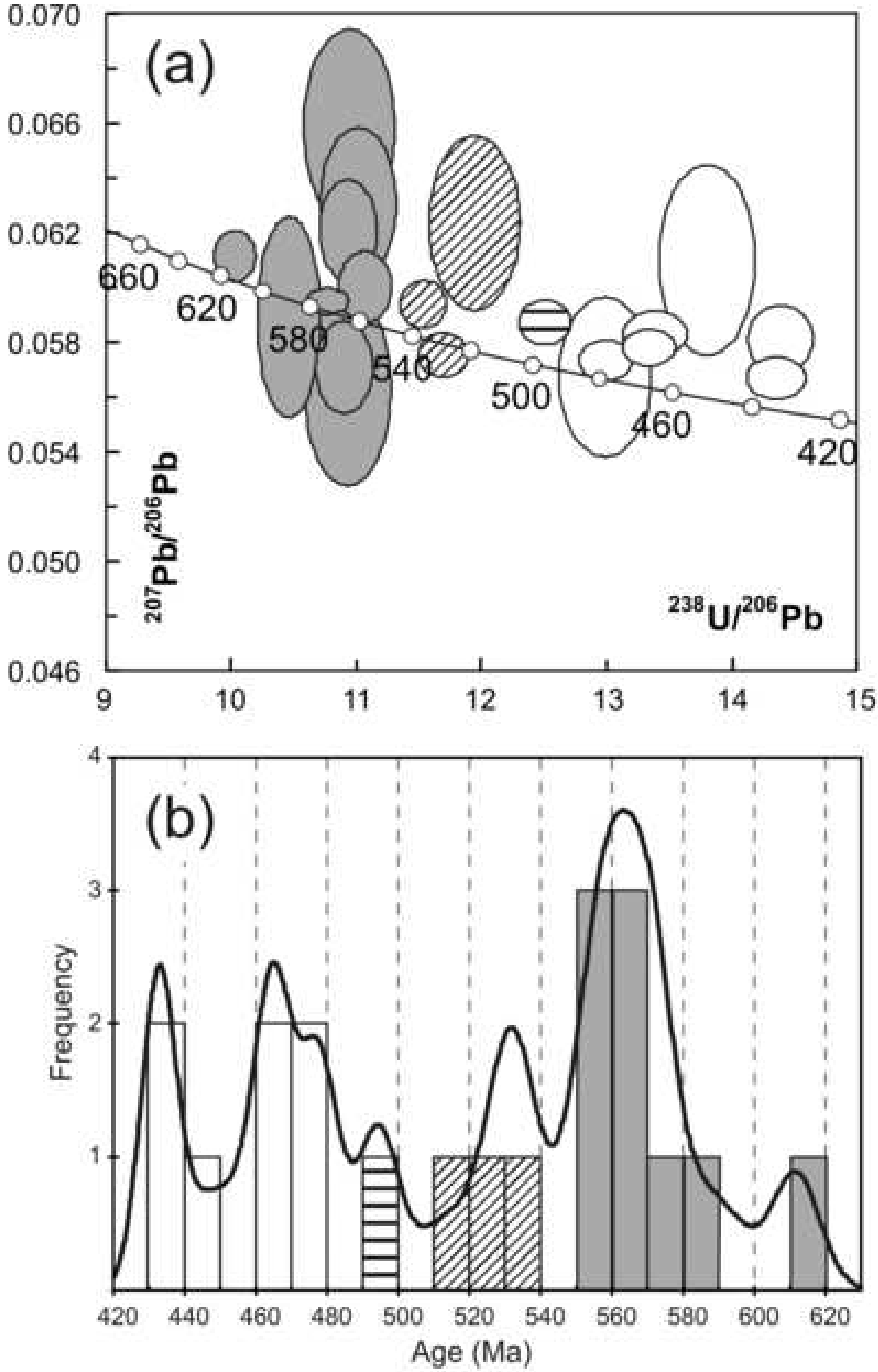

Fig 10

Figure
Click here to download high resolution image

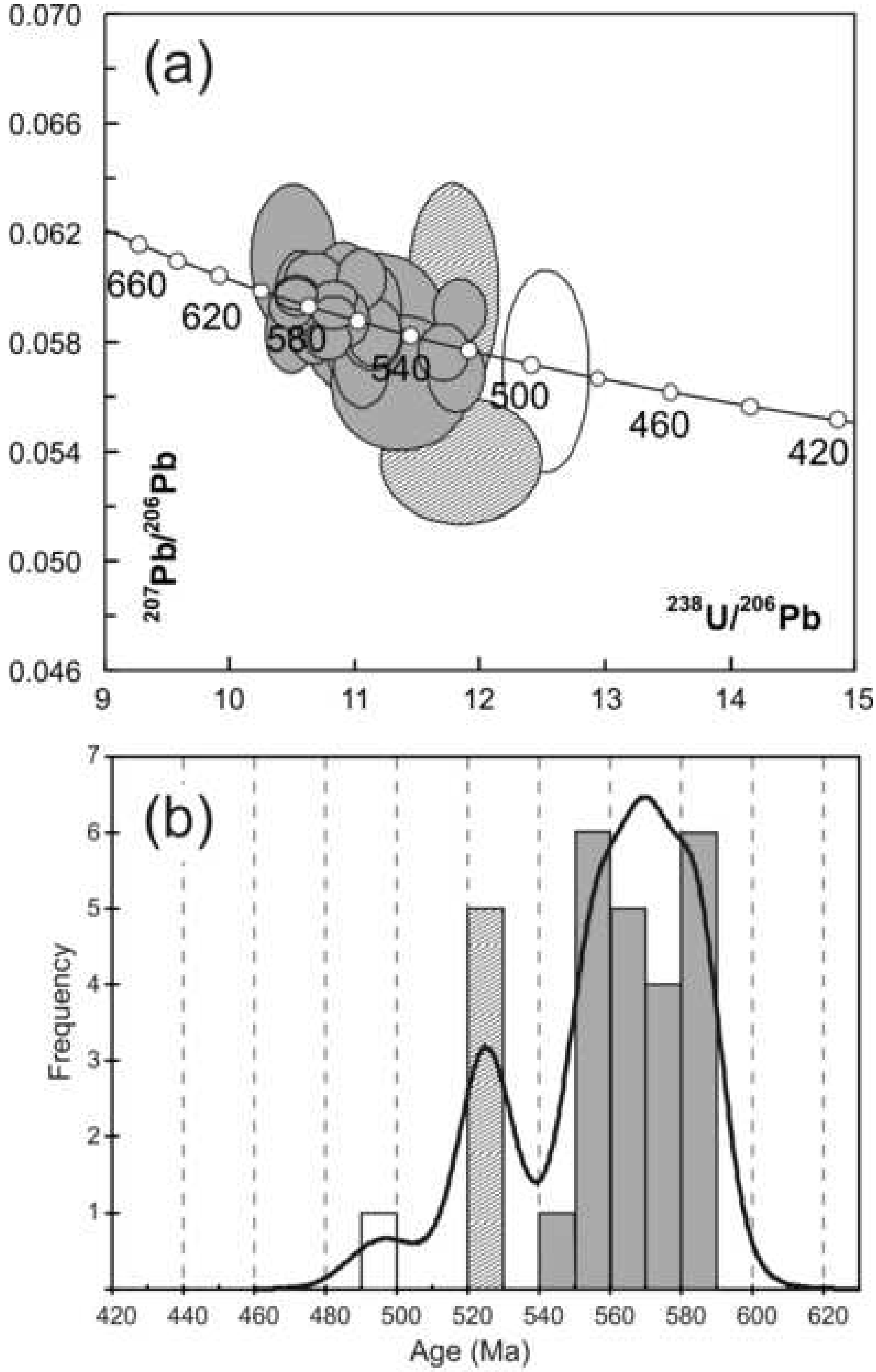

Fig 11

Figure
Click here to download high resolution image

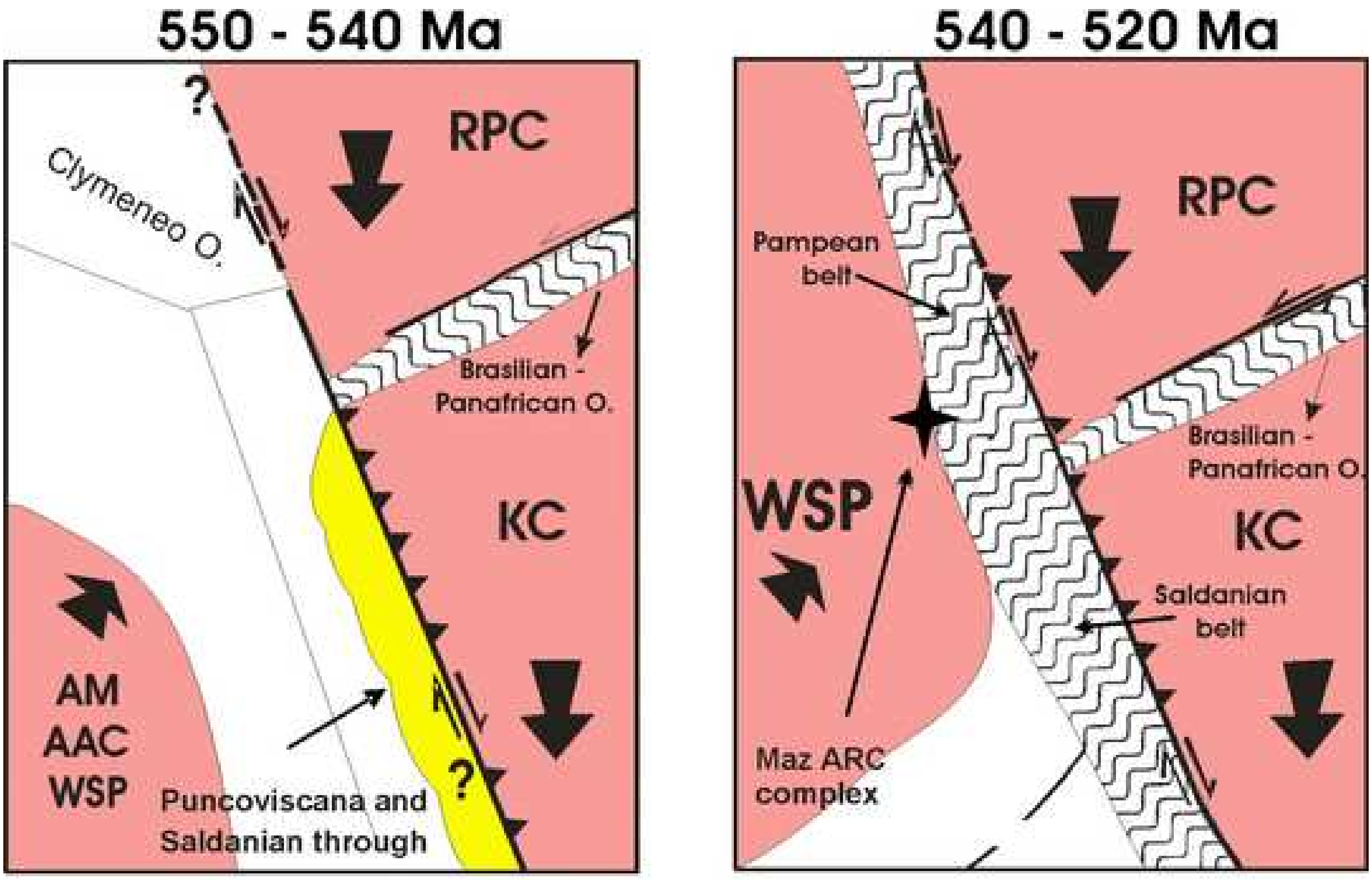

Fig. 12

Sample	MAZ-12061	MAZ-12061	MAZ-12061	MAZ-12091	MAZ-12091	MAZ-12091	MAZ-12091	MAZ-12086
Analysis	10	11	9	2	4	5	8	11
Mineral	apatite	apatite	apatite	apatite	apatite	apatite	apatite	apatite
SiO2								
FeO	0.25	0.15	0.11	0.13	0.16	0.13	0.16	0.13
MnO	0.22	0.24	0.20	0.12	0.07	0.16	0.13	0.13
MgO	0.01	bdl	bdl	0.03	bdl	bdl	bdl	bdl
CaO	54.08	53.89	54.12	54.97	55.73	55.29	55.61	52.71
Na2O	0.29	0.28	0.24	0.13	0.09	0.13	0.10	0.49
K2O	bdl	bdl	bdl	0.02	bdl	bdl	0.01	0.00
P2O5	41.44	41.43	41.61	41.85	42.10	41.38	42.04	40.52
F	2.64	2.71	2.65	2.98	2.38	2.37	2.44	2.76
Cl	bdl	bdl	bdl	bdl	bdl	bdl	bdl	0.06
Total	98.93	98.70	98.92	100.22	100.53	99.46	100.48	96.78
CO2±OH	1.07	1.30	1.08	bdl	bdl	0.54	bdl	3.22
Fe2	0.017	0.01	0.007	0.009	0.011	0.009	0.011	0.009
Mn	0.016	0.017	0.014	0.008	0.005	0.011	0.009	0.009
Mg	0.001	0	0	0.003	0	0	0	
Sr	0	0	0	0	0	0	0	
Ca	4.751	4.745	4.748	4.78	4.806	4.83	4.802	4.742
Na	0.046	0.044	0.039	0.02	0.014	0.021	0.015	0.079
K	0	0	0	0.002	0	0	0.001	
Si	0	0	0	0	0	0	0	
P	2.877	2.882	2.885	2.875	2.869	2.856	2.868	2.88
S	0	0	0	0	0	0	0	
Cations	7.708	7.698	7.693	7.697	7.705	7.727	7.706	7.719
CF	1.37	1.408	1.372	1.527	1.211	1.222	1.242	1.466
CCl	0	0	0	0.016	0.016	0.016	0.016	0.016
O	*12*	*12*	*12*	*12*	*12*	*12*	*12*	*12*